replenishment rate of readily releasable vesicles (Toonen et al., 2006), suggesting that heterozygous deletion of *Stxbp1* indeed affected synaptic function in mice. It is possible that the absence of seizures in *Stxbp1* heterozygous knockout mice might be due to the different genetic background. Because *Stxbp1* mutants have been backcrossed for at least six generations to a C57BL/6 background (Toonen et al., 2006), it would be interesting to examine whether seizures would occur in other genetic background. Alternatively, effect of gene dosage alterations of *STXBP1/Stxbp1* may vary between humans and mice: Humans might be more susceptible than mice; therefore, loss of function of one allele could cause seizures only in humans but not in mice. Appropriate mice models by neatly manipulating gene dosage of *Stxbp1* may mimic human phenotype and enable detailed analysis of pathogenesis of infantile epileptic encephalopathy in relation to impaired synaptic function.

Acknowledgments

We would like to thank patients and their families for their participation in this study. We would like to thank Dr. Sean Megason for the pCIR vector. This work was supported by Research Grants from the Ministry of Health, Labour and Welfare (N.M. and M.K.), Grant-in-Aid for Scientific Research on Priority Areas-(Research on Pathomechanisms of Brain disorder)-from the Ministry of Education, Culture, Sports, Science and Technology of Japan (N. M.), Grant-in-Aid for Scientific Research from Japan Society for the Promotion of Science (N.M. and M.K.), Grant-in-Aid for Young Scientist from Japan Society for the Promotion of Science (H.S.), Research Promotion Fund from Yokohama Foundation for Advancement of Medical Science (H.S.), Research Promotion Fund from The Uehara Memorial Foundation (H.S.), Research Grants from the Japan Epilepsy Research Foundation (H.S. and M.K.), Grant for 2009 Strategic Research Project of Yokohama City University (H.S.), and Research Grant from Naito Foundation (N.M.).

Disclosure

We confirm that we have read the Journal's position on issues involved in ethical publication and affirm that this report is consistent with those guidelines. None of the authors has any conflict of interest to disclose.

References

Bahi-Buisson N, Nectoux J, Rosas-Vargas H, Milh M, Boddaert N, Girard B, Cances C, Ville D, Afenjar A, Rio M, Heron D, N'Guyen Morel MA, Arzimanoglou A, Philippe C, Jonveaux P, Chelly J, Bienvenu T. (2008) Key clinical features to identify girls with CDKL5 mutations. *Brain* 131:2647–2661.

Ciufo LF, Barclay JW, Burgoyne RD, Morgan A. (2005) Munc18-1 regulates early and late stages of exocytosis via syntaxin-independent protein interactions. *Mol Biol Cell* 16:470–482.

Djukic A, Lado FA, Shinnar S, Moshe SL. (2006) Are early myoclonic encephalopathy (EME) and the Ohtahara syndrome (EIEE) independent of each other? *Epilepsy Res* 70(suppl 1):S68–S76.

Engel J Jr. (2006) Report of the ILAE classification core group. *Epilepsia* 47:1558–1568.

Guerrini R, Moro F, Kato M, Barkovich AJ, Shiihara T, McShane MA, Hurst J, Loi M, Tohyama J, Norci V, Hayasaka K, Kang UJ, Das S, Dobyns WB. (2007) Expansion of the first PolyA tract of ARX causes infantile spasms and status dystonicus. *Neurology* 69:427–433.

Hamdan FF, Piton A, Gauthier J, Lortie A, Dubeau F, Dobrzeniecka S, Spiegelman D, Noreau A, Pellerin S, Cote M, Henrion E, Fombonne E, Mottron L, Marineau C, Drapeau P, Lafreniere RG, Lacaille JC, Rouleau GA, Michaud JL. (2009) De novo STXBP1 mutations in mental retardation and nonsyndromic epilepsy. *Ann Neurol* 65: 748–753.

Kalscheuer VM, Tao J, Donnelly A, Hollway G, Schwinger E, Kubart S, Menzel C, Hoeltzenbein M, Tommerup N, Eyre H, Harbord M, Haan E, Sutherland GR, Ropers HH, Gecz J. (2003) Disruption of the serine/threonine kinase 9 gene causes severe X-linked infantile spasms and mental retardation. *Am J Hum Genet* 72:1401–1411.

Kato M, Das S, Petras K, Sawaishi Y, Dobyns WB. (2003) Polyalanine expansion of ARX associated with cryptogenic West syndrome. *Neurology* 61:267–268.

Kato M. (2006) A new paradigm for West syndrome based on molecular and cell biology. *Epilepsy Res* 70(suppl 1):S87–S95.

Kato M, Saitoh S, Kamei A, Shiraishi H, Ueda Y, Akasaka M, Tohyama J, Akasaka N, Hayasaka K. (2007) A longer polyalanine expansion mutation in the ARX gene causes early infantile epileptic encephalopathy with suppression-burst pattern (Ohtahara syndrome). *Am J Hum Genet* 81:361–366.

Maquat LE, Kinniburgh AJ, Rachmilewitz EA, Ross J. (1981) Unstable beta-globin mRNA in mRNA-deficient beta o thalassemia. *Cell* 27:543–553.

Ohtahara S, Ishida T, Oka E, Yamatogi Y, Inoue H, Karita S, Ohtsuka Y. (1976) [On the specific age dependent epileptic syndrome: the early-infantile epileptic encephalopathy with suppression-burst.]. *No to Hattatsu* 8:270–279.

Ohtahara S, Yamatogi Y. (2006) Ohtahara syndrome: with special reference to its developmental aspects for differentiating from early myoclonic encephalopathy. *Epilepsy Res* 70(suppl 1):S58–S67.

Saitsu H, Kato M, Mizuguchi T, Hamada K, Osaka H, Tohyama J, Uruno K, Kumada S, Nishiyama K, Nishimura A, Okada I, Yoshimura Y, Hirai S, Kumada T, Hayasaka K, Fukuda A, Ogata K, Matsumoto N. (2008) *De novo* mutations in the gene encoding STXBP1 (MUNC18-1) cause early infantile epileptic encephalopathy. *Nat Genet* 40:782–788.

Shyu AB, Wilkinson MF, van Hoof A. (2008) Messenger RNA regulation: to translate or to degrade. *EMBO J* 27:471–481.

Stromme P, Mangelsdorf ME, Shaw MA, Lower KM, Lewis SM, Bruyere H, Lutcherath V, Gedeon AK, Wallace RH, Scheffer IE, Turner G, Partington M, Frints SG, Fryns JP, Sutherland GR, Mulley JC, Gecz J. (2002) Mutations in the human ortholog of Aristaless cause X-linked mental retardation and epilepsy. *Nat Genet* 30:441–445.

Toonen RF, Wierda K, Sons MS, de Wit H, Cornelisse LN, Brussaard A, Plomp JJ, Verhage M. (2006) Munc18-1 expression levels control synapse recovery by regulating readily releasable pool size. *Proc Natl Acad Sci U S A* 103:18332–18337.

Verhage M, Maia AS, Plomp JJ, Brussaard AB, Heeroma JH, Vermeer H, Toonen RF, Hammer RE, van den Berg TK, Missler M, Geuze HJ, Sudhof TC. (2000) Synaptic assembly of the brain in the absence of neurotransmitter secretion. *Science* 287:864–869.

Weaving LS, Christodoulou J, Williamson SL, Friend KL, McKenzie OL, Archer H, Evans J, Clarke A, Pelka GJ, Tam PP, Watson C, Lahooti H, Ellaway CJ, Bennetts B, Leonard H, Gecz J. (2004) Mutations of CDKL5 cause a severe neurodevelopmental disorder with infantile spasms and mental retardation. *Am J Hum Genet* 75: 1079–1093.

Yamatogi Y, Ohtahara S. (2002) Early-infantile epileptic encephalopathy with suppression-bursts, Ohtahara syndrome; its overview referring to our 16 cases. *Brain Dev* 24:13–23.

Supporting Information

Additional Supporting Information may be found in the online version of this article:

Table S1. PCR conditions and primer sequences.

Please note: Wiley-Blackwell is not responsible for the content or functionality of any supporting materials supplied by the authors. Any queries (other than missing material) should be directed to the corresponding author for the article.

Disrupted *SOX10* Regulation of *GJC2* Transcription Causes Pelizaeus-Merzbacher-Like Disease

Hitoshi Osaka, MD, PhD,[1,2]
Haruka Hamanoue, MD, PhD,[3]
Ryoko Yamamoto, MSc,[4]
Atsuo Nezu, MD, PhD,[5] Megumi Sasaki, BA,[4]
Hirotomo Saitsu, MD, PhD,[3]
Kenji Kurosawa, MD, PhD,[6]
Hiroko Shimbo, MP,[1]
Naomichi Matsumoto, MD, PhD,[3]
and Ken Inoue, MD, PhD[4]

Mutations in the gap junction protein gamma-2 gene, *GJC2*, cause a central hypomyelinating disorder; Pelizaeus-Merzbacher-like disease (PMLD; MIM311601). Using a homozygosity mapping and positional candidate gene approach, we identified a homozygous mutation (c.-167A>G) within the *GJC2* promoter at a potent SOX10 binding site in a patient with mild PMLD. Functionally, this mutation completely abolished the SOX10 binding and attenuated *GJC2* promoter activity. These findings suggest not only that the *SOX10*-to-*GJC2* transcriptional dysregulation is a cause of PMLD, but also that *GJC2* may be in part responsible for the central hypomyelination caused by *SOX10* mutations.

ANN NEUROL 2010;68:250–254

Congenital hypomyelinating disorders are a heterogeneous group of central nerve system (CNS) leukoencephalopathies, most of which are inherited disorders of myelin formation. The prototype condition is Pelizaeus-Merzbacher disease (PMD; MIM312080), an X-linked disorder caused by mutations in the proteolipid protein 1 gene (*PLP1*).[1] Patients with PMD have nystagmus, impaired motor development, ataxia, choreoathetotic movements, dysarthria, and progressive spasticity. However, ~20 to 50 % of patients clinically diagnosed with PMD have no detectable abnormalities in the *PLP1* gene, and some have a distinct disease, Pelizaeus-Merzbacher-like disease (PMLD; MIM311601).

Mutations in the gap junction protein gamma-2 gene (*GJC2*, also known as *Cx47* or *GJA12*) have been reported as a cause of PMLD.[2–8] Twenty-four different mutations (8 frameshift, 10 missence, 5 nonsense, and 1 missense/insertion alterations) have been reported to date, and most if not all result in a loss of channel function.[7,9]

By combining homozygosity mapping and a candidate gene approach, we found a homozygous mutation that disrupts a SOX10 transcriptional activation site in the *GJC2* promoter region in a family showing a mild PMLD phenotype. SOX10 is an high mobility group (HMG) family transcription factor that plays a critical role in peripheral nervous system (PNS) and CNS myelination. In addition, a subset of *SOX10* mutations cause peripheral and central hypomyelination, Waardenburg syndrome, and Hirschsprung disease (PCWH; MIM609136).[10] This study reports the first case of PMLD caused by a mutation in the *GJC2* promoter and suggests that *SOX10* transcriptional regulation of *GJC2* plays a critical role in CNS myelination.

Patients and Methods

Detailed clinical information of a Japanese female patient with PMLD, who is now 25-years-old, was previously reported.[11] In brief, her healthy parents were second cousins. She had congenital pendular nystagmus as a neonate, but otherwise developed normally and was educated at a normal school. At the age of 10 years, she developed a spastic gait that worsened and made her wheelchair bound by the age of 12 years. Her disease progressed to mild athetosis of the upper limbs and ataxia by age 13 years and dysarthria by age 15 years. She cannot speak and understands only easy commands now. Brain magnetic resonance imaging at age 15 and 20 years showed diffuse hyperintensity of white matter on T2-weighted images with interval progression of brain atrophy (Fig 1). Electrophysiological examinations showed extensive nerve conduction slowing in the CNS, although this was less severe than usually seen in male patients with PMD.[11] Peripheral nerve conduction velocities were nor-

From the [1]Division of Neurology, Clinical Research Institute, Kanagawa Children's Medical Center; [2]Molecular Pathology and Genetics Division, Kanagawa Cancer Center Research Institute; [3]Department of Human Genetics, Yokohama City University Graduate School of Medicine; [4]Department of Mental Retardation and Birth Defect Research, National Institute of Neuroscience, National Center of Neurology and Psychiatry, Kodaira; [5]Division of Pediatric Neurology, Yokohama Ryoiku-iryo Center; and [6]Division of Genetics, Clinical Research Institute, Kanagawa Children's Medical Center, Yokohama, Japan.

Address correspondence to Dr Osaka, Division of Neurology, Clinical Research Institute, Kanagawa Children's Medical Center, Yokohama, 232-855, Japan. E-mail: hosaka@kcmc.jp

Additional Supporting Information can be found in the online version of this article.

Received Dec 29, 2009, and in revised form Jan 29, 2010. Accepted for publication Feb 26, 2010.

Published online in Wiley InterScience (www.interscience.wiley.com). DOI: 10.1002/ana.22022

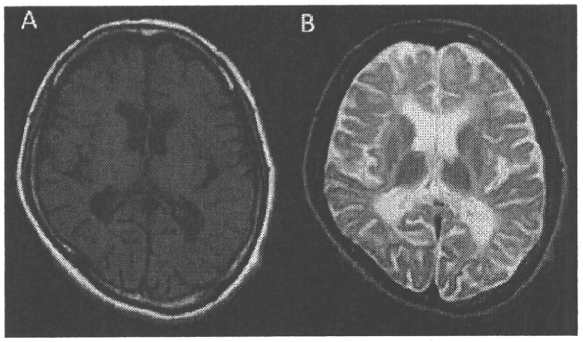

FIGURE 1: Magnetic resonance imaging of the cerebrum. (A) T1-weighted image of the proband at 20 years shows cerebral atrophy with ventricular dilatation and widening of a subarachnoidal space. Disappearance of contrast between cortex and white matter, which suggested incomplete myelination throughout the cerebrum, was evident. (B) T2-weighted image reveals diffuse hyperintensity in the white matter, suggesting the arrest of myelination. Note that the inner capsule, which is usually myelinated in the neonate, was not myelinated in this patient.

mal. Molecular examinations excluded *PLP1* exonic mutations, large duplications, and deletions.

Informed consent was obtained from the patient and family members in accordance with human study protocols approved by the institutional review board of Kanagawa Children's Medical Center. Genomic DNA was extracted from peripheral lymphocytes. A genome-wide single nucleotide polymorphism (SNP) genotyping was undertaken for III-1, III-3, IV-1, IV-2, V-1, and V-2 (Fig 2A) using the GeneChip Human Mapping 10K Array *X*ba 142 2.0 (Affymetrix, Santa Clara, CA) containing 10,204 SNPs according to the manufacture's protocols (Supplementary Materials and Methods). Polymerase chain reaction and DNA sequencing are described in the Supplementary Materials and Methods (Supplementary Table 1).

Mammalian cell expression plasmids for the wild-type and E189X mutant human *SOX10* cDNA were reported previously.[12] Luciferase reporter plasmids containing mouse *Gjc2* promoters (kindly provided from Dr M. Wegner) were utilized

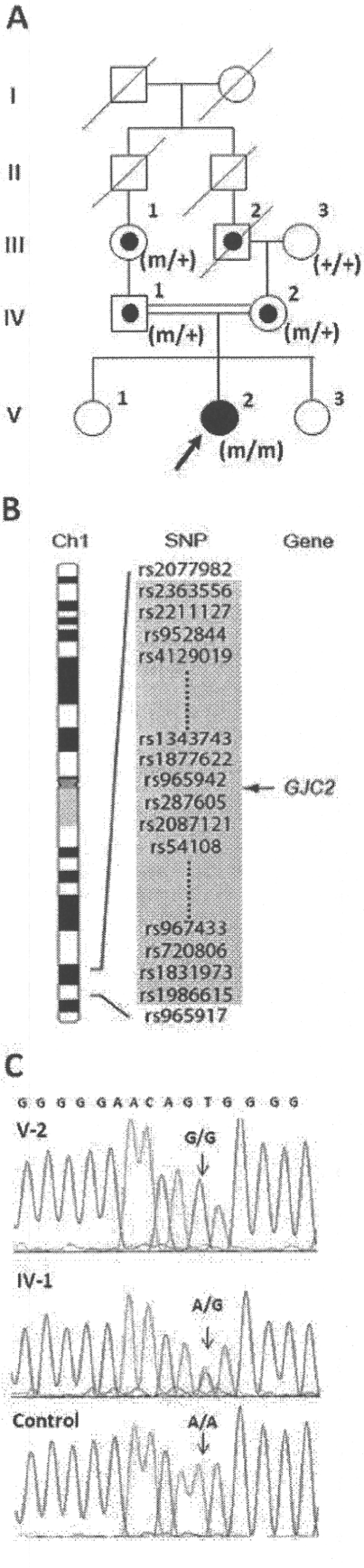

FIGURE 2: Family pedigree, largest region of interest on chromosome 1, and the *CJC2* mutation. (A) Pedigree of the Pelizaeus-Merzbacher-like disease family with the proband *(filled circle with arrow)*. DNA from III-1, III-3, IV-1, IV-2, V-1, and V-2 were used for single nucleotide polymorphism (SNP) genotyping. Carriers are indicated as circles with black dots. m = mutant allele; + = wild-type allele. (B) The largest region of interest by homozygosity SNP mapping at 1q41-q42.2. The homozygous interval is shown as a shaded square with SNP identifiers. The location of *GJC2* is shown with an arrow. The region between rs2077982 and rs965917 was 18.2 Mb in size (University of California, Santa Cruz genome browser coordinate, chromosome 1: 215150317-233384165, February 2009 version). (C) Sequencing chromatograms from the patient (V-2, top), a carrier (IV-1, middle), and a normal control (bottom). The c.-167A>G mutation in the promoter region of *CJC2* is shown with arrows.

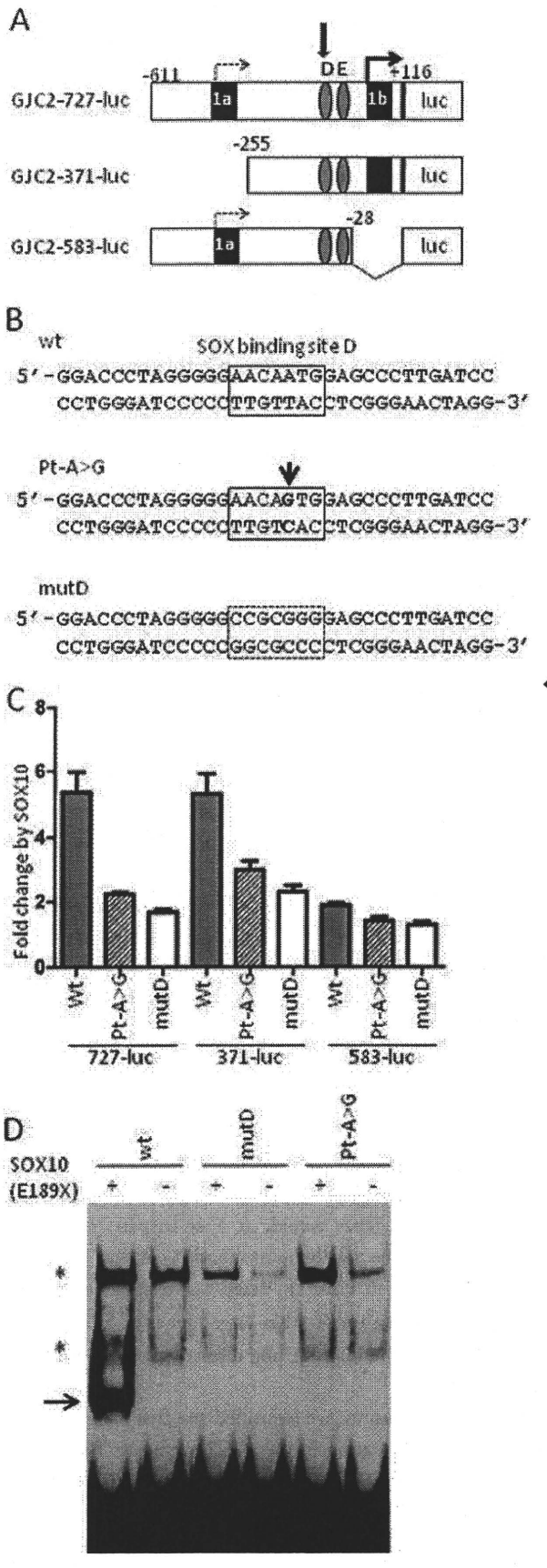

for site-directed mutagenesis (see Supplementary Materials and Methods). We measured *GJC2* transcriptional activity by luciferase reporter assays using human glioblastoma U138 cells (see Supplementary Materials and Methods). SOX10 binding affinity was determined by electrophoretic mobility shift assay (EMSA) using synthetic oligonucleotide probes and nuclear extracts from HeLa cells transfected with pCMV-SOX10-E189X, as previously described.[13]

Results

The largest region with homozygosity identified by SNP genotyping on chromosome 1q42.13 was our primary focus for candidate gene scanning (see Fig 2B, Supplementary Table 2, Supplementary Fig 1). Among 115 refseq genes mapped within this region, 34 gene products were identified from mouse whole brain proteomics studies (Supplementary Table 3).[14,15] After we sequenced all coding regions and intron-exon boundaries of these 34 genes to exclude any disease-causing mutations, we extended our analysis to promoter regions. We found a homozygous mutation, c.-167A>G, in the proximal promoter re-

FIGURE 3: Functional consequence of the c.-167A>G point mutation in the *GJC2* promoter. (A) Schematic diagram of the luciferase reporter constructs of mouse *Gjc2* promoter region utilized in this study. Exon 1b contains the major transcription start site *(thick arrow)*, whereas exon 1a contains the minor site *(dotted arrow)*. GJC2-727-luc contains a full proximal promoter, whereas GJC2-371-luc lacks exon 1a and the upstream portion and GJC2-583-luc lacks exon 1b. Two SOX10 binding site, D and E, are shown as shaded ovals with a thick arrow pointing to site D, where the mutation was identified. (B) Sequences of the probes used for electrophoretic mobility shift assays (EMSAs). Top: *wt* probe containing the wild-type site D *(square)*. Middle: Pt-A>G probe carrying c.-167A>G mutation *(arrow)*. Bottom: mutD probe in which site D was changed to abolish SOX10 binding. (C) Transcriptional activities of different *GJC2* promoter constructs carrying either wt, Pt-A>G, or mutD at site D shown as fold changes obtained by presence or absence of SOX10 determined by luciferase reporter assay. Note that the *wt* constructs for 727-luc and 371-luc, harboring the major start site in exon 1b, were activated by SOX10 >5-fold. In contrast, a much smaller effect was observed when either Pt-A>G or mutD was introduced. The 583-luc constructs, which only harbor a minor transcription start site, remain inactivated by SOX10 regardless of changes in site D. Each bar represents average ± standard deviation. Each experiment was performed 3×, each in triplicate. Results from a representative experiment were shown. (D) DNA binding affinity of each probe (shown in B) was determined by EMSA using nuclear extracts from HeLa cells transfected with plasmid expressing truncated SOX10 protein (E189X) or empty plasmid (as a negative control). The *wt* probe showed a strong binding to E189X SOX10 protein, which retains enhanced DNA binding ability *(arrow)*. In contrast, we observed no binding of the mutant probes, either mutD or Pt-A>G. Asterisks show nonspecific binding. Free probes were observed at the bottom of the picture.

gion of *GJC2* that segregated with PMLD in the family members (see Fig 2A and C) and was absent in 122 normal Japanese chromosomes. Analysis of this region in 10 additional female PMLD patients without mutations in the open reading frame of *GJC2* detected no abnormalities.

Interestingly, this mutation is located within a critical SOX10 binding site (designated as site D) in the syntenic mouse *Gjc2* proximal promoter and diminishes the consensus of the SOX binding sequence (AACAATG to AACAGTG, Fig 3A and B). Based on this, we predicted that this mutation disrupts *GJC2* promoter activity and measured transcription in vitro using a luciferase reporter system. Because the region harboring the mutation is highly conserved across mammals,[16] we introduced this mutation into well-studied mouse *Gjc2* promoter constructs (see Fig 3A and B). The c.-167A>G point mutation in the SOX10 binding site dramatically decreased transcription to levels similar to a completely disrupted SOX10 binding site D (see Fig 3C). These findings suggest that the c.-167A>G point mutation found in our patients results in a diminished *GJC2* transcription.

Based on these results, we hypothesized that this mutation altered SOX10 binding affinity to site D and tested this by EMSA. Because full-length SOX10 has a low binding affinity that is difficult to distinguish from background noise, we used a C-terminus truncation version of SOX10, E189X, which retains the HMG binding domain and has enhanced binding affinity.[16] Introduction of the c.-167A>G mutation into site D resulted in a complete loss of E189X SOX10 binding (see Fig 3D). Therefore, combined with the preceding observations, we find that the c.-167A>G mutation abolishes SOX10 binding to the *GJC2* promoter, resulting in a dramatic attenuation of the *GJC2* transcription.

Discussion

GJC2 encodes Cx47, a member of the connexin family. Connexins are components of gap junctions, intercellular channels that allow ions and small molecules to pass across neighboring plasma membranes. Gap junctions have diverse functions, including the propagation of electrical signals and metabolic cooperation. Two hemichannels, each built up of 6 connexin protein subunits on opposing cell membranes, form the channel. Astrocytes and oligodendrocytes are coupled by gap junctions constructed predominantly of GJC2 (Cx47) and Cx43.[17] Because Cx47 proteins carrying PMLD-causing mutations either fail to reach the membrane or have reduced transport activity, loss of function is likely the mechanism underlying the CNS hypomyelination in PMLD.[7,9] Herein we report the first *GJC2* promoter mutation,[18] c.-167A>G, in a patient with PMLD, and this is associated with allelic transcription failure.

Our female patient had nystagmus, spasticity, and choreoathetosis, clinical symptoms common to PMD and PMDL. However, she attained normal motor and intellectual developmental milestones. Because only $\frac{1}{3}$ (11 of 33) of PMLD patients with *GJC2* mutations have walked unsupported,[2–7] her clinical manifestation was mild and overlaps with that of spastic paraplegia phenotype. Of note, she lost her motor and cognitive abilities within a few years, accompanied by progressive brain atrophy (see Fig 1). Such acute regression has rarely been observed in PMD and is more characteristic of PMLD secondary to *GJC2* mutations.[6]

A recent study showed that SOX10 directly regulates *GJC2* by binding to its proximal promoter.[16] Site D, the SOX10 binding site in which our mutation was identified, plays a predominant role in *GJC2* promoter activity,[16] and the c.-167A>G mutation we identified reduces its affinity for SOX10 and abolishes *GJC2* transcription. These findings suggest that *SOX10* regulation of *GJC2* via site D is essential for proper *GJC2* expression and that its failure causes PMLD. Presumably, the relatively milder clinical phenotype observed in our patient results from reduced but not completely abolished transcriptional activity, allowing translation of a small amount of normal Cx47 protein.

This constitutes the second disorder associated with dysregulation of a SOX10 target gene. Previously, mutations within the *SOX10* binding site of the *GJB1* promoter have been shown to cause demyelinating peripheral neuropathy.

Together the peripheral neuropathy and PMLD provide a partial understanding of the clinical manifestations of PCWH patients. Because these patients have SOX10 mutations,[10] we predict that the expression of both *GJC2* and *GJB1* is impaired. Impaired expression of both of these genes would, at least in part, respectively account for the de-/hypomyelination of the CNS and PNS observed in PCWH. Based on this, we predict that impaired expression of other target genes of SOX10 is responsible for the Hirschprung disease and other Waardenburg features.

In conclusion, we identified the first case of PMLD caused by a mutation in the *GJC2* promoter. Because this mutation disrupts SOX10 regulation of *GJC2* transcription, we hypothesize that SOX10 regulation of transcription plays a major role in nervous system myelination.

Acknowledgments

This study was supported by grants-in-aid for scientific research from the Ministry of Education, Culture, Sports, Science, and Technology, Japan (H.O., K.I.), Takeda Science Foundation (H.O.), Yokohama Foundation for Advancement of Medical Science (H.O.), and Kanagawa children's hospital (K.K., H.O.), and Health Labor Sciences Research Grants from the Ministry of Health, Labor, and Welfare, Japan (H.O., K.K., N.M., K.I.).

We thank Dr M. Wegner for kindly providing us plasmid DNAs and Drs C. Boerkoel, C. du Souich, and P. Atkins for their critical reviews.

Potential Conflicts of Interest

Nothing to report.

References

1. Inoue K. PLP1-related inherited dysmyelinating disorders: Pelizaeus-Merzbacher disease and spastic paraplegia type 2. Neurogenetics 2005;6:1–16.
2. Uhlenberg B, Schuelke M, Ruschendorf F et al. Mutations in the gene encoding gap junction protein alpha 12 (connexin 46.6) cause Pelizaeus-Merzbacher-like disease. Am J Hum Genet. 2004;75:251–260.
3. Bugiani M, Al Shahwan S, Lamantea E et al. GJA12 mutations in children with recessive hypomyelinating leukoencephalopathy. Neurology. 2006;67:273-279.
4. Wolf NI, Cundall M, Rutland P et al. Frameshift mutation in GJA12 leading to nystagmus, spastic ataxia and CNS dys-/demyelination. Neurogenetics. 2007;8:39–44.
5. Salviati L, Trevisson E, Baldoin MC et al. A novel deletion in the GJA12 gene causes Pelizaeus-Merzbacher-like disease. Neurogenetics. 2007;8:57-60.
6. Henneke M, Combes P, Diekmann S et al. GJA12 mutations are a rare cause of Pelizaeus-Merzbacher-like disease. Neurology. 2008;70:748-754.
7. Orthmann-Murphy JL, Salsano E, Abrams CK et al. Hereditary spastic paraplegia is a novel phenotype for GJA12/GJC2 mutations. Brain. 2009;132:426–438.
8. Wang J, Wang H, Wang Y et al. Two novel gap junction protein alpha 12 gene mutations in two Chinese patients with Pelizaeus-Merzbacher-like disease. Brain Dev. 2009; doi:10.1016/j.braindev.2009.03.013.
9. Orthmann-Murphy JL, Enriquez AD, Abrams CK, Scherer SS. Loss-of-function GJA12/Connexin47 mutations cause Pelizaeus-Merzbacher-like disease. Mol Cell Neurosci. 2007;34:629–641.
10. Pingault V, Bondurand N, Kuhlbrodt K et al. SOX10 mutations in patients with Waardenburg-Hirschsprung disease. Nat Genet. 1998;18:171-173.
11. Nezu A, Kimura S, Uehara S et al. Pelizaeus-Merzbacher-like disease: female case report. Brain Dev. 1996;18:114–118.
12. Inoue K, Khajavi M, Ohyama T et al. Molecular mechanisms for distinct neurological phenotypes conveyed by allelic truncating mutations. Nat Genet. 2004;36:361–369.
13. Inoue K, Ohyama T, Sakuragi Y et al. Translation of SOX10 3' untranslated region causes a complex severe neurocristopathy by generation of a deleterious functional domain. Hum Mol Genet. 2007;16:3037–3046.
14. Taylor CM, Marta CB, Claycomb RJ et al. Proteomic mapping provides powerful insights into functional myelin biology. Proc Natl Acad Sci U S A. 2004;101:4643–4648.
15. Wang H, Qian WJ, Chin MH et al. Characterization of the mouse brain proteome using global proteomic analysis complemented with cysteinyl-peptide enrichment. J Proteome Res. 2006;5:361–369.
16. Schlierf B, Werner T, Glaser G, Wegner M. Expression of connexin47 in oligodendrocytes in regulated by the Sox10 transcription factor. J Mol Biol. 2006;361:11–21.
17. Orthmann-Murphy JL, Freidin M, Fischer E et al. Two distinct heterotypic channels mediate gap junction coupling between astrocyte and oligodendrocyte connexins. J Neurosci. 2007;27:13949–13957.
18. Ruf N, Uhlenberg B. Analysis of human alternative first exons and copy number variation of the GJA12 gene in patients with Pelizaeus-Merzbacher-like disease. Am J Med Genet B Neuropsychiatr Genet. 2009;150B:226–232.
19. Bondurand N, Girard M, Pingault V et al. Human Connexin 32, a gap junction protein altered in the X-linked form of Charcot-Marie-Tooth disease, is directly regulated by the transcription factor SOX10. Hum Mol Genet. 2001;10:2783-2795.
20. Houlden H, Girard M, Cockerell C et al. Connexin 32 promoter P2 mutations: a mechanism of peripheral nerve dysfunction. Ann Neurol. 2004;56:730–734.

Amantadine is thought to partially increase dopamine release and inhibit glutamatergic activity by blocking the NMDA receptor. Bupropion, an atypical antidepressant of the aminoketone class, increases the reuptake of norepinephrine and dopamine (but not serotonin), and can also act as a nicotinic antagonist. Hence, as both drugs raise the dopamine level in the synaptic cleft, dopamine might be mediating the myoclonus. Alternatively (or additionally), amantadine and bupropion could exert the same effect by acting on different neurotransmitter systems that converge onto a single functional neuronal network. Their possible interactions[4,5] and subsequent signaling consequences[6] will depend on the relative location of the involved neurotransmitter receptors.[7]

LEGENDS TO THE VIDEO

Segment 1A. Shows the patient on amantadine with spontaneous and speech-activated myoclonus in the platysma and perioral muscles (orbicularis oculi, mentalis, depressor labii inferioris), as well as involving the eye lids.

Segment 1B. Shows the patient after cessation of amantadine. The action myclonus of the face has resolved, allowing for normalization of speech.

Segment 2A. Shows the patient on bupropion. Speech-activated myoclonus in platysma and buccinator muscles (more prominent on the right side) causes stuttering and involuntary pausing during speech, particularly seen in the last 30 seconds of the video clip. Additionally, as described by the patient, myoclonus in her upper limbs is seen.

Segment 2B. Shows the patient off bupropion. Myoclonus of the lower face (and upper limbs) has resolved, restoring her speech.

Author Roles: AG and AEL: Conception and design, manuscript writing and editing.

Amitabh Gupta, MD, PhD
Anthony E. Lang, MD, FRCPC*
Movement Disorders Unit, Toronto Western Hospital
University of Toronto, Ontario, Canada
**E-mail: lang@uhnres.utoronto.ca*

References

1. Pfeiffer RF. Amantadine-induced "vocal" myoclonus. Mov Disord 1996;11:104–106.
2. Frucht S, Fahn S. The clinical spectrum of posthypoxic myoclonus. Mov Disord 2000;15(Suppl 1):2–7.
3. Gelfand JM, Nelson AB, Fross RD, Glass GA. Speech-activated myoclonus masquerading as stuttering. Neurology 2009;72:1964.
4. Brotchie JM. Nondopaminergic mechanisms in levodopa-induced dyskinesia. Mov Disord. 2005;20:919–931.
5. Placzek AN, Zhang TA, Dani JA. Age dependent nicotinic influences over, dopamine neuron synaptic plasticity. Biochem Pharmacol 2009;78:686–692.
6. Lee FJ, Xue S, Pei L, et al. Dual regulation of NMDA receptor functions by direct protein-protein interactions with the dopamine D1 receptor. Cell 2002;111:219–230.
7. Balla A, Nattini ME, Sershen H, Lajtha A, Dunlop DS, Javitt DC. GABAB/NMDA receptor interaction in the regulation of extracellular dopamine levels in rodent prefrontal cortex and striatum. Neuropharmacology 2009;56:915–921.

Choreo–Ballistic Movements in a Case Carrying a Missense Mutation in Syntaxin Binding Protein 1 Gene

Video 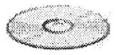

Early infantile epileptic encephalopathy (EIEE), also called Ohtahara syndrome, is an epileptic syndrome characterized with seizure onset within the first 2 to 3 months after birth, tonic spasms in an isolated form or in a series, suppression–bursts on the electroencephalography (EEG), and poor prognosis with severe mental and motor retardation. The syndrome is often associated with structural brain damage. A few cases with metabolic disorders have also been reported.[1] Some cases are cryptogenic in which genetic factors may be involved.[2] Recently, *syntaxin binding protein 1* (*STXBP1*) mutations were identified in individuals with cryptogenic EIEE.[3] We describe a case of EIEE, carrying a missense mutation in *STXBP1*, who developed severe choreo–ballism.

A 10-year-old boy was admitted to our hospital with the chief complaint of severe automatic involuntary movements (AIMs). The parents and the 2 siblings were healthy, and there was no family history of AIMs. The patient had no perinatal complications. He developed EIEE 2 months after birth, which evolved into West syndrome. He continued to have frequent tonic seizures and started to manifest vigorous AIMs at the age of 5 years. Seizures and AIMs were intractable, and he had to be placed on high-dose phenobarbital. He showed profound psychomotor developmental delay.

Paroxysmal AIMs, involving the face, neck, and extremities were repeated at short intervals in the awake state (Supporting Information Video), never appearing during sleep. The AIMs showed a stereotypical pattern. Quick orofacial movements, such as grimacing and mouth opening, and abrupt head rotations were observed. The AIMs in his extremities were proximally dominant and flinging with torsive components. Jerky flexion and extension of the fingers, wrists, and toes were also observed. The AIMs were induced by tactile stimuli and were suppressed when a part of his body, such as the upper or lower extremities, was wrapped with cloth. The nature of his AIMs was consistent with choreo–ballism. EEGs in the sleep (Fig. 1A) and awake (Fig. 1B) states showed continuous multifocal spikes and spike-wave complexes, maximal in bilateral occipital, and posterior temporal areas. No change in electrical activity was observed preceding or during the AIMs (Fig. 1B). Tc99m ECD single-photon emission computed tomography in the awake state showed a decreased uptake of Tc99m in the bilateral frontotemporal lobes, both with and without AIMs. No increase in Tc99m uptake was observed with AIMs in the cingulate gyrus or in other areas. These results confirmed

Additional Supporting Information may be found in the online version of this article.

Financial disclosure: Nothing to report.
Potential conflict of interest: Nothing to report.
Published online 18 August 2010 in Wiley Online Library (wileyonlinelibrary.com). DOI: 10.1002/mds.23164

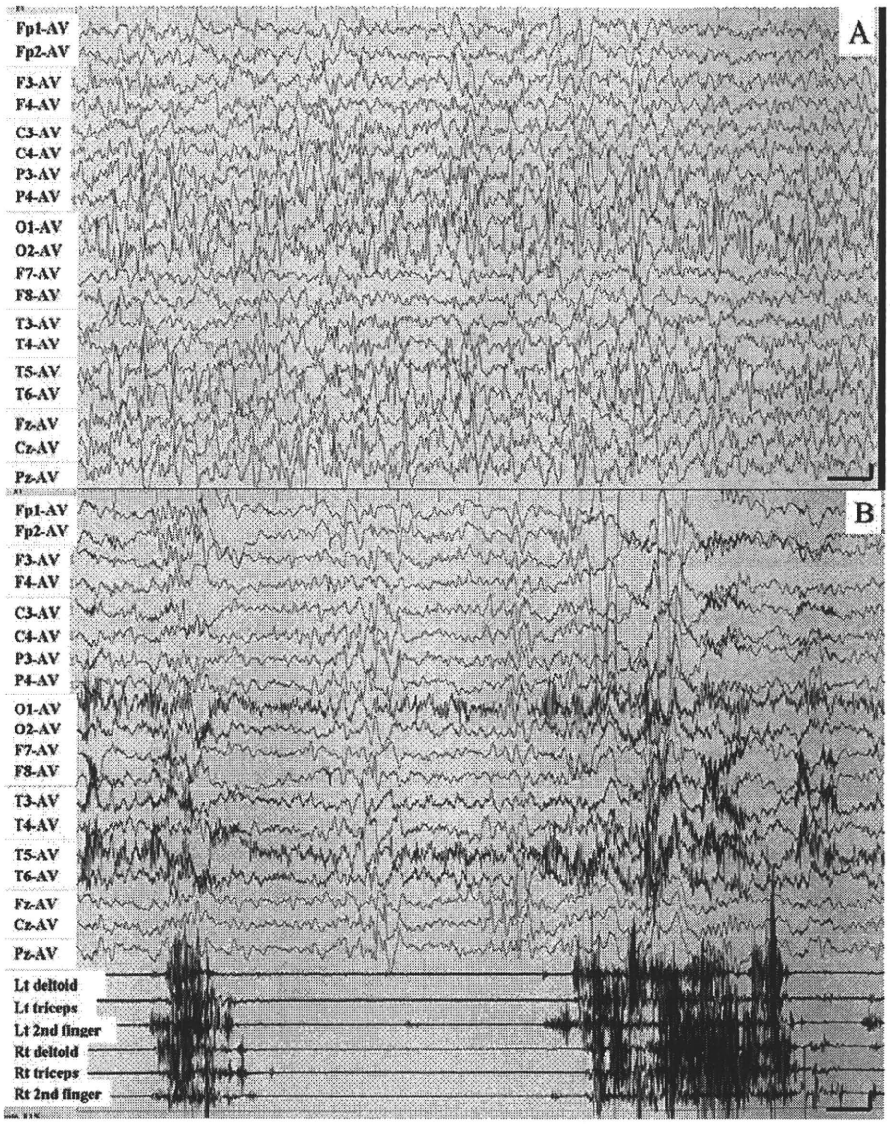

FIG. 1. **A**: Sleep EEGs. **B**: EEGs in the awake state with surface electromyography. EEGs in the awake state showed no change in electrical activity, whether it was accompanied by AIMs or not. Sensitivity 20 μV/mm. AV, average.

that his AIMs were not epileptic seizures, including those originating from the cingulate cortex.

Brain MRI showed no structural anomalies. Blood chemistry, lactate and pyruvate in blood and cerebrospinal fluid (CSF), amino acids in plasma and urine, and organic acids in urine, lysosomal enzyme activities, and chromosome G-banding were within normal limits. CSF analysis including homovanillic acid, 5-hydroxyindolacetic acid, and methoxyhydroxyphenylglycol showed no abnormalities. Ophthalmological examinations were normal. The case was considered as a cryptogenic EIEE. However, he has recently been shown to have a heterozygous missense mutation 251T→A(V84D) in *STXBP1*, at 9q34.11.[3]

STXBP1, a neuronal Sec1/Munc-18 protein, controls fusion between synaptic vesicles and the presynaptic plasma membrane and plays a central role in synaptic neurotransmitter release.[4] In 2008, defects in *STXBP1* were identified in 5 individuals with cryptogenic EIEE, including the present case.[3] Hamdan et al.[5] subsequently identified mutations in *STXBP1* in 2 patients with severe mental retardation (MR) and non-EIEE epilepsy. Impaired synaptic vesicle release

caused by *STXBP1* haploinsufficiency is speculated to contribute to the pathogenesis of epilepsy and MR.

The present case is remarkable because he developed vigorous choreo–ballism subsequent to EIEE. Such severe AIMs in an EIEE case have not been previously reported, and no movement disorders including choreo–ballism were recognized in the other 4 cases reported by Saitsu et al.[3,6] Interestingly, the 2 cases reported by Hamdan et al.,[5] however, manifested diffuse tremor.[5] The pathogenesis of chorea and ballism is considered to involve dysfunction of the indirect pathway in the motor loop, which connects the basal ganglia, thalamus, and motor cortex.[7] The dysfunction of the motor loop including the basal ganglia has also been associated with the pathogenesis of tremor. As the pathways are regulated by excitatory and inhibitory neurotransmitters, such as dopamine, glutamate, and GABA, aberrant neurotransmitter release caused by *STXBP1* mutations may well be a cause of basal ganglia disorders as well as epilepsy and MR. The observation in the present case, however, is not a final proof of causality. The clinical features of *STXBP1* mutations have not been determined due to a limited number of cases reported. This disorder, however, may give an important clue to the common molecular pathophysiology of epilepsy, MR, and basal ganglia diseases.

Legends to the Video

The AIMs start in the left fingers and spread to the face, neck, and extremities. The AIMs of the extremities are of a flinging nature with torsive components. They stereotypically repeat at short intervals.

Author Roles: Kyoko Kanazawa: conception and design, data acquisition and analysis, drafting, and revising of the text. Satoko Kumada: conception and design, data acquisition and analysis, and revision of the text. Mitsuhiro Kato: data analysis and revising of the text. Hirotomo Saitsu: Data acquisition and drafting of the text. Eiji Kurihara: conception and design, and revising of the text. Naomichi Matsumoto: data acquisition and drafting of the text.

Kyoko Kanazawa, MD*
Satoko Kumada, MD, PhD
Department of Neuropediatrics
Tokyo Metropolitan Neurological Hospital
Tokyo, Japan
**E-mail: brisedemer-ezweb@umin.ac.jp*

Mitsuhiro Kato, MD, PhD
Department of Pediatrics
Yamagata University School of Medicine
Yamagata, Japan

Hirotomo Saitsu, MD, PhD
Department of Human Genetics
Yokohama City University Graduate School of Medicine
Yokohama, Japan

Eiji Kurihara, MD
Department of Neuropediatrics
Tokyo Metropolitan Neurological Hospital
Tokyo, Japan

Naomichi Matsumoto, MD, PhD
Department of Human Genetics
Yokohama City University Graduate School of Medicine
Yokohama, Japan

References

1. Aicardi J, Ohtahara S. Severe neonatal epilepsies with suppression-burst pattern. In: Roger J, Bureau M, Dravet C, Genton P, Tassinari CA, Wolf P, editors. Epileptic syndromes in infancy, childhood and adolescence. Montrouge: John Libbey Eurotext; 2005. p 39–50.
2. Kato M, Saitoh S, Kamei A, et al. A longer polyalanine expansion mutation in the ARX gene causes early infantile epileptic encephalopathy with suppression-burst pattern (Ohtahara syndrome). Am J Hum Genet 2007;81:361–366.
3. Saitsu H, Kato M, Mizuguchi T, et al. De novo mutations in the gene encoding STXBP1 (MUNC18-1) cause early infantile epileptic encephalopathy. Nat Genet 2008;40:782–788.
4. Gerst JE. SNAREs and SNARE regulators in membrane fusion and exocytosis. Cell Mol Life Sci 1999;55:707–734.
5. Hamdan FF, Piton A, Gauthier J, et al. De novo STXBP1 mutations in mental retardation and nonsyndromic epilepsy. Ann Neurol 2009;65:748–753.
6. Tohyama J, Akasaka N, Osaka H, et al. Early onset West syndrome with cerebral hypomyelination and reduced cerebral white matter. Brain Dev 2008;30:349–355.
7. Alexander GE, Crutcher MD. Functional architecture of basal ganglia circuits: neural substrates of parallel processing. Trends Neurosci 1990;13:266–271.

CLINICAL GENETICS
An International Journal of Genetics, Molecular, and Personalized Medicine

Clin Genet 2010
Printed in Singapore. All rights reserved

CLINICAL GENETICS
doi: 10.1111/j.1399-0004.2010.01575.x

Short Report

Paternal mosaicism of an *STXBP1* mutation in OS

Saitsu H, Hoshino H, Kato M, Nishiyama K, Okada I, Yoneda Y, Tsurusaki Y, Doi H, Miyake N, Kubota M, Hayasaka K, Matsumoto N. Paternal mosaicism of an *STXBP1* mutation in OS. Clin Genet 2010. © John Wiley & Sons A/S, 2010

Ohtahara syndrome (OS) is one of the most severe and earliest forms of epilepsy. We have recently identified that the *de novo* mutations of *STXBP1* are important causes for OS. Here we report a paternal somatic mosaicism of an *STXBP1* mutation. The affected daughter had onset of spasms at 1 month of age, and interictal electroencephalogram showed suppression-burst pattern, leading to the diagnosis of OS. She had a heterozygous c.902+5G>A mutation of *STXBP1*, which affects donor splicing of exon 10, resulting in 138-bp insertion of intron 10 sequences in the transcript. The mutant transcript had a premature stop codon, and was degraded by nonsense-mediated mRNA decay in lymphoblastoid cells derived from the patient. High-resolution melting analysis of clinically unaffected parental DNAs suggested that the father was somatic mosaic for the mutation, which was also suggested by sequencing. Cloning of PCR products amplified with the paternal DNA samples extracted from blood, saliva, buccal cells, and nails suggested that 5.3%, 8.7%, 11.9%, and 16.9% of alleles harbored the mutation, respectively. This is a first report of somatic mosaicism of an *STXBP1* mutation, which has implications in genetic counseling of OS.

Conflict of interest

None of the authors has any conflict of interest to disclose.

H Saitsu[a], H Hoshino[b], M Kato[c], K Nishiyama[a], I Okada[a], Y Yoneda[a], Y Tsurusaki[a], H Doi[a], N Miyake[a], M Kubota[b], K Hayasaka[c] and N Matsumoto[a]

[a]Department of Human Genetics, Yokohama City University Graduate School of Medicine, Fukuura 3-9, Kanazawa-ku, Yokohama 236-0004, Japan, [b]Division of Neurology, National Center for Child Health and Development, Okura 2-10-1, Setagaya-ku, Tokyo 157-8535, Japan, and [c]Department of Pediatrics, Yamagata University Faculty of Medicine, Iida-nishi 2-2-2, Yamagata 990-9585, Japan

Key words: HRM analysis – OS – somatic mosaicism – *STXBP1*

Corresponding author: Dr Hirotomo Saitsu, Department of Human Genetics, Yokohama City University Graduate School of Medicine, 3-9 Fukuura, Kanazawa-ku, Yokohama 236-0004, Japan.
Tel.: +81-45-787-2606;
fax: +81-45-786-5219;
e-mail: hsaitsu@yokohama-cu.ac.jp

Received 8 August 2010, revised and accepted for publication 30 September 2010

Ohtahara syndrome (OS), also known as early infantile epileptic encephalopathy with suppression-burst, is one of the most severe and earliest forms of epilepsy (1). It is characterized by early onset of seizures, typically frequent epileptic spasms, seizure intractability, characteristic suppression-burst patterns on electroencephalogram (EEG), and poor outcome with severe psychomotor retardation (2, 3). Brain malformations such as cerebral dysgenesis or hemimegalencephaly are often associated with OS, but cryptogenic or idiopathic OS is found in a subset of OS patients, in whom genetic aberrations might be involved (4). Mutations in *ARX* gene have been found in several male patients with OS (5–8). We have recently found *de novo* mutations in *STXBP1* (encoding syntaxin binding protein 1, also known as MUNC18-1) in individuals with cryptogenic OS (9). A microdeletion involving *STXBP1* and various kinds of point mutations including missense, frameshift, nonsense, and splicing mutations have been found in about one-third of Japanese cases with cryptogenic OS (10). We have showed that both missense mutations and

a splicing mutation result in haploinsufficiency of *STXBP1*: degradation of STXBP1 proteins with missense mutations and nonsense-mediated mRNA decay (NMD) associated with an aberrantly spliced mRNAs (10).

Here we describe a family with an affected daughter with an *STXBP1* mutation and healthy parents. Parental analysis indicates that the father is somatic mosaic for the mutation. Detailed molecular analysis is presented.

Materials and methods

Patient and her parents

The 1-year-old girl is a product of unrelated healthy parents. There is no history of epilepsy in her parents. She was born at term without asphyxia after an uneventful pregnancy. Her physical and neurological findings were normal until vomitting, which was supposed to be a presymptomatic event of seizures, was observed at 25 days of age, and her seizures started at 37 days of age, consisting of brief tonic spasms, occasionally in cluster, followed by vomiting and subtle seizures, such as head extension, upward eye gazing, and vocalization, with increased muscle tone of her extremities for a few seconds. According to suppression-burst pattern on EEG (Fig. 1a,b), she was diagnosed as OS. Brain magnetic resonance imaging (MRI) showed normal brain structure (Fig. 1c–f). Seizures were refractory to antiepileptic drugs, such as high-dose phenobarbital, phenytoin, zonisamide, pyridoxal phosphate, valproic acid, ketogenic diet, and potassium bromide. Injection of adrenocorticotropic hormone (ACTH) was partially effective. She was hypertonic and could not control her head or smile. At 6 months of age, a mild rigospastic quadriplegia was noted. Developmental milestones were profoundly delayed.

DNA samples

Peripheral blood leukocytes from the patient and her parents as well as other tissues from the father were used for this study. Genomic DNA from whole blood, saliva, buccal cells, and nails were isolated using a Wizard Genomic DNA Purification Kit (Promega, Tokyo, Japan), an Oragene DNA kit (DNA Genotek, Ottawa, Canada), an ISOHAIR kit (Nippon Gene, Toyama, Japan), and a Gentra Puregene Buccal Cell Kit (Gentra, Minneapolis, MN), respectively. Experimental protocols were approved by Institutional Review Boards for Ethical Issues at Yokohama City University School of Medicine and Yamagata University Faculty of Medicine. Informed consent was obtained from the patient's parents in agreement with the requirements of Japanese regulations.

Mutation analysis and TA cloning

Mutation screening of *STXBP1* by high-resolution melting (HRM) analysis using RotorGene-6200 HRM (Corbett Life Science, Brisbane, Australia) was performed as previously described (10). Parentage was confirmed by microsatellite analysis (9). For measurement of the ratio of wild-type and mutant alleles, PCR products using paternal DNA as a template were subcloned into pCR4-TOPO vector (Invitrogen, Carlsbad, CA). Cloned fragments were amplified with PCR mixture containing 1 × ExTaq buffer, 0.2 mM each dNTP, 0.5 μM each primer, and 0.375 U Ex TaqHS polymerase (Takara Bio, Ohtsu, Japan). M13 forward (5′-TAAAACGACGGCCAGTGAAT-3′) and M13 reverse (5′-CAGGAAACAGCTATGACCAT GA-3′) primers were used for amplification, and an ex10-F (5′-AGCTGAAGAGGGTTCGAT GA-3′) primer was used for sequencing.

RNA analysis

RNA analysis using lymphoblastoid cells (LCL) was performed essentially as previously described (10). Briefly, after incubation with dimethyl sulfoxide (as vehicle control) or 30 μM cycloheximide (Sigma, Tokyo, Japan) for 4 h, total RNA was extracted using RNeasy Plus Mini Kit (Qiagen, Tokyo, Japan). Two micrograms total RNA was subjected to reverse transcription, and 1 μl cDNA was used for PCR. Primer sequences are ex9-F (5′-CCCTGTGCTCCATGAATTGAC TTT-3′) and ex12-R (5′-CTGAGGCATCTTCTTC AGCATCTGG-3′). Inhibition of NMD was estimated according to the density ratios of lower normal and upper aberrant bands with/without 30-μM cycloheximide treatments in the culture of the patient's LCL. Two separately extracted RNA samples were used for duplicated experiments, respectively. Data were averaged and the standard deviation was calculated. Statistical analyses were performed using the unpaired Student's *t*-test (two-tailed). DNA of each PCR band purified by QIAEXII Gel extraction kit (Qiagen, Tokyo, Japan) was sequenced.

Results

Through the screening for *STXBP1* mutations in individuals with cryptogenic OS, we found a patient harboring heterozygous c.902+5G>A mutation. To examine whether the mutation

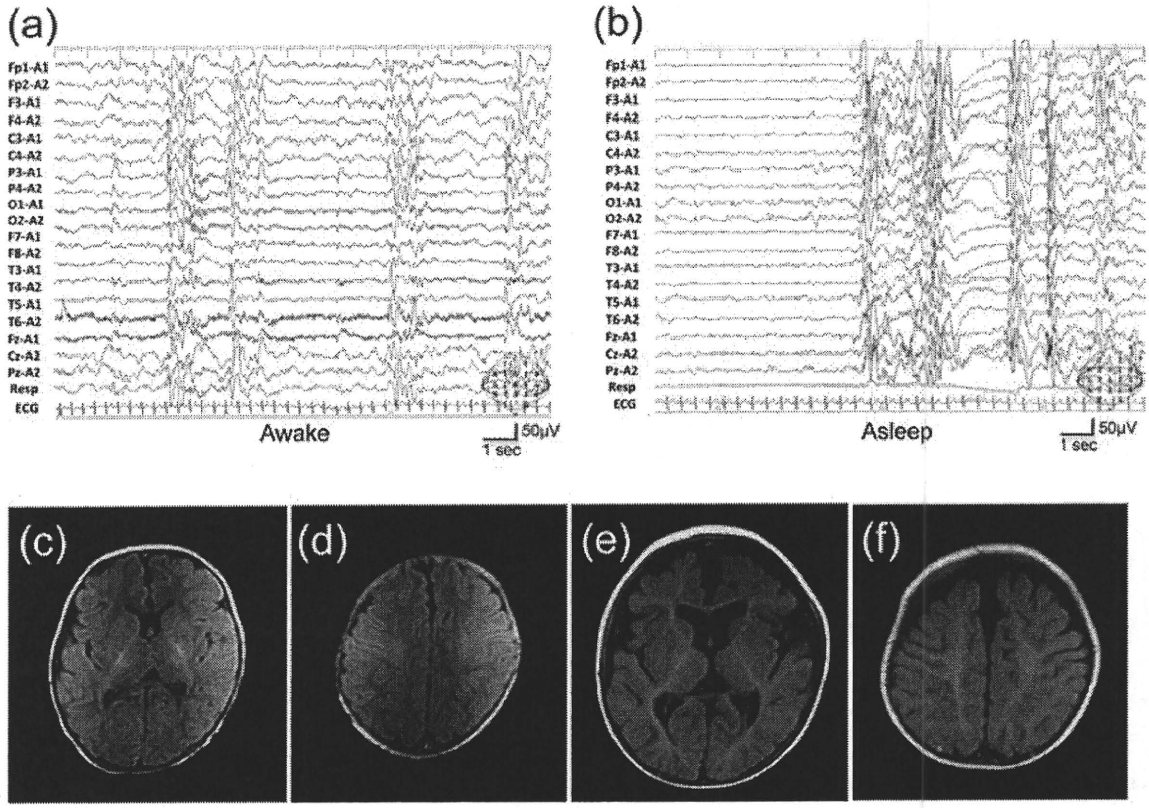

Fig. 1. Interictal electroencephalogram (EEG) (**a, b**) and brain magnetic resonance imaging (MRI) (**c–f**) of the patient. EEG during both waking (**a**) and sleep (**b**) at 1 month of age showed suppression-burst pattern consisting of low-voltage, almost flat phase and high-voltage paroxysmal activity phase. Brain MRI showed normal findings at 1 month of age (**c, d**), and slightly dilated lateral ventricles at 11 months of age (**e, f**) because of adrenocorticotropic hormone injection.

could affect donor splicing of exon 10, reverse transcriptase (RT)–PCR designed to amplify exons 9–12 was performed using total RNA extracted from LCL derived from the patient (Fig. 2a). A single band (286 bp), corresponding to the wild-type *STXBP1* allele, was amplified using a cDNA template from a control LCL (Fig. 2b). By contrast, a longer band was detected from the patient's cDNA (Fig. 2b). The longer mutant transcript had a 138-bp insertion of intron 10 sequences (Fig. 2c), producing a premature stop codon at amino acid position 302; therefore, the mutant mRNAs are probably to be degraded by NMD (11, 12). The intensity ratio of the mutant compared to the normal band was increased up to 36.3% after treatment with 30 μM cycloheximide, which inhibits NMD, compared to 13.8% in the untreated condition (Fig. 2d). Thus the mutant transcript suffered from degradation by NMD, which would result in haploinsufficiency of *STXBP1*.

To examine whether the c.902+5G>A mutation occurred *de novo*, the parental DNA extracted from whole blood were analyzed by HRM. Compared with the mother's sample, the patient's sample showed clearly shifted melting curve, indicating that the heterozygous c.902+5G>A mutation could be surely detected (Fig. 3a). Interestingly, the father's sample showed a slightly shifted melting curve, suggesting that the father may harbor the mutation in mosaic state, which was suggested by sequencing (Fig. 3a,b). Similar melting curves and electropherograms were obtained in DNA extracted from saliva, buccal cells, and nails (Fig. 3a,b). We further investigated the mosaicism by counting wild-type G and mutant A alleles after TA cloning of the PCR product. DNA extracted from blood, saliva, buccal cells, and nails suggested that 5.3%, 8.7%, 11.9%, and 16.9% of alleles (i.e. 10.6%, 17.4%, 23.8%, and 33.8% of cells) harbored the mutation, respectively (Fig. 3c).

Discussion

To date, 13 point mutations and one deletion of *STXBP1* have been reported in individuals with OS (9, 10). Thirteen out of fourteen deletion/mutations were confirmed as *de novo* events (paternal DNA was unavailable for one

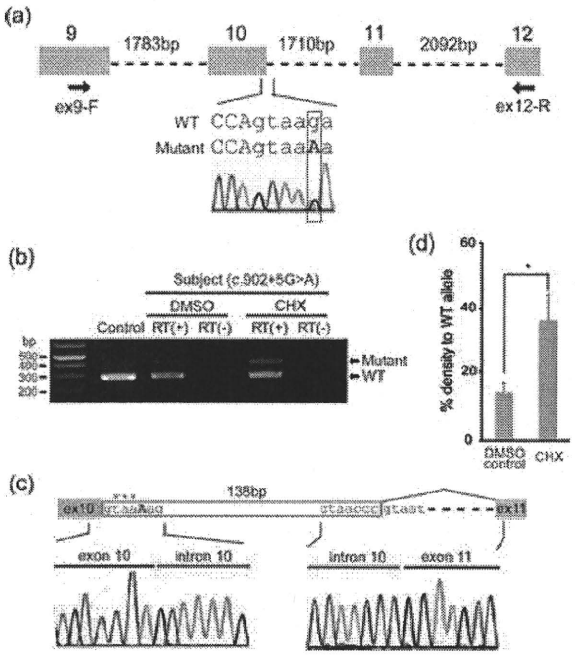

Fig. 2. The c.902+5G>A mutation causing abnormal splicing associated with nonsense-mediated mRNA decay (NMD). (**a**) Schematic representation of the genomic structure from exons 9 to 12 of *STXBP1*. Exons, introns and primers are shown by gray boxes, dashed lines and arrows, respectively. The mutation in intron 10 was colored in red. Sequences of exon and intron are presented in upper and lower cases, respectively. (**b**) Reverse transcriptase (RT) – PCR analysis of the patient with c.902+5G>A and a normal control. Two PCR products were detected from the patient's cDNA: lower was the wild-type (WT) transcript and upper was the mutant. Only a single WT amplicon was detected in a control. The mutant amplicon was significantly increased by 30-μM cycloheximide (CHX) treatment compared to DMSO treatment as a vehicle control. RT (+): with reverse transcriptase, RT (−): without reverse transcriptase as a negative control. (**c**) Sequence of mutant amplicons clearly showed a 138-bp insertion of intron 10 sequences and a premature stop codon (asterisk) in the mutant transcript. (**d**) Quantitative analysis of the NMD inhibition by CHX based on the data shown in (**b**). *p = 0.00186 by unpaired Student's *t*-test (two-tailed). Averages of duplicated experiments using two distinctive RNA samples, respectively, are shown with error bars (standard deviation).

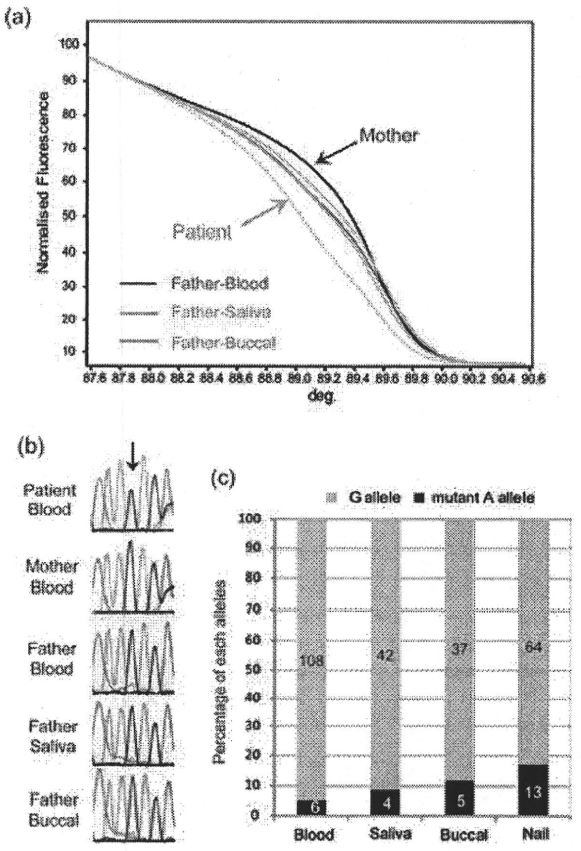

Fig. 3. Paternal somatic mosaicism of the c.902+5G>A mutation. (**a**) Melting curves of PCR products. Compared with the mother's sample (black), the patient's sample (gray) showed largely shifted melting curve. The father's sample from blood (red), saliva (green), and buccal cells (blue) showed slightly, but distinctly shifted melting curves. (**b**) Electropherograms of the c.902+5G>A mutation (arrow) showed mosaicism of the mutation in the father. (**c**) Allele frequencies counted by TA cloning of PCR products and sequencing. DNA extracted from blood, saliva, buccal cells, and nails of the father showed that 5.3%, 8.7%, 11.9%, and 16.9% of alleles harbored the mutant A allele. The numbers of colonies corresponding to each allele are indicated within bars.

remaining mutation). Many OSs are sporadic, probably because of their poor outcome with severe psychomotor retardation; however, some X-linked familial cases have been reported with *ARX* mutations (6, 8). Here we have showed a paternal somatic mosaicism of an *STXBP1* mutation. Although DNA from the semen of the father could not be analyzed in this study, the identical c.902+5G>A mutation found in both the father and the affected daughter indicated that the father should possess the mutation in germ cells as a mosaic state, suggesting recurrence risks. Thus, somatic and germline mosaicism of *STXBP1* mutations should be carefully taken into account especially for genetic counseling of familial OS cases.

We have successfully identified the paternal somatic mosaicism of an *STXBP1* mutation by HRM. DNA from blood indicated that the mosaic ratio is as low as about 5%; therefore, HRM could be very sensitive in detecting low-ratio mosaicism. HRM is a rapid and simple approach to detect heteroduplexes (13). It only requires the addition of a saturating dye before PCR. By HRM analysis of the PCR products, the sensitivity of successful detection of heterozygotes is nearly 100% (13). It should be noted that the sensitivity of HRM to detect somatic changes or heteroplasmy is much

better than that of DNA sequencing (14, 15): HRM could detect the level of somatic mosaicism down to 5–10% (15). However, the ability to detect low percentage heterodeuplex of PCR products may vary among mutations. Although the heterozygous c.902+5G>A mutation showed largely shifted melting curve, we experienced some heterozygous mutations only showing slightly shifted melting curve, in which we may not be able to detect the mosaicism. Therefore, optimization of HRM analysis for each mutation would be recommended especially to examine parental samples.

In conclusion, we firstly described the paternal somatic mosaicism of an *STXBP1* mutation. The percentage of mosaicism was quite low (5–17%), and no minor problems like dexterity, intelligence (cognition), behavior or psychological state were recognized in the father. The information described here was quite useful for future genetic counseling of this family.

Acknowledgements

We would like to thank the patient and her family for their participation in this study. This work was supported by Research Grants from the Ministry of Health, Labour and Welfare (N. M. and M. K.), Grant-in-Aid for Scientific Research from Japan Society for the Promotion of Science (N. M. and M. K.), Grant-in-Aid for Young Scientist from Japan Society for the Promotion of Science (H. S.), Research Promotion Fund from Yokohama Foundation for Advancement of Medical Science (H. S.), Research Grants from the Japan Epilepsy Research Foundation (H. S. and M. K.), and Research Grant from Naito Foundation (N. M.).

References

1. Ohtahara S, Ishida T, Oka E et al. On the specific age dependent epileptic syndrome: the early-infantile epileptic encephalopathy with suppression-burst. No to Hattatsu 1976: 8: 270–279.
2. Djukic A, Lado FA, Shinnar S et al. Are early myoclonic encephalopathy (EME) and the Ohtahara syndrome (EIEE) independent of each other?. Epilepsy Res 2006: 70 (Suppl. 1): S68–S76.
3. Ohtahara S, Yamatogi Y. Ohtahara syndrome: with special reference to its developmental aspects for differentiating from early myoclonic encephalopathy. Epilepsy Res 2006: 70 (Suppl. 1): S58–S67.
4. Yamatogi Y, Ohtahara S. Early-infantile epileptic encephalopathy with suppression-bursts, Ohtahara syndrome; its overview referring to our 16 cases. Brain Dev 2002: 24: 13–23.
5. Kato M, Saitoh S, Kamei A et al. A Llonger Ppolyalanine Eexpansion Mmutation in the ARX Ggene Ccauses Eearly Iinfantile Eepileptic Eencephalopathy with Ssuppression-Bburst Ppattern (Ohtahara Ssyndrome). Am J Hum Genet 2007: 81: 361–366.
6. Fullston T, Brueton L, Willis T et al. Ohtahara syndrome in a family with an ARX protein truncation mutation (c.81C>G/p.Y27X). Eur J Hum Genet 2010: 18: 157–162.
7. Absoud M, Parr JR, Halliday D et al. A novel ARX phenotype: rapid neurodegeneration with Ohtahara syndrome and a dyskinetic movement disorder. Dev Med Child Neurol 2009: 52: 305–307.
8. Kato M, Koyama N, Ohta M et al. Frameshift mutations of the ARX gene in familial Ohtahara syndrome. Epilepsia 2010: 51: 1679–1684.
9. Saitsu H, Kato M, Mizuguchi T et al. *De novo* mutations in the gene encoding STXBP1 (MUNC18-1) cause early infantile epileptic encephalopathy. Nat Genet 2008: 40: 782–788.
10. Saitsu H, Kato M, Okada I et al. STXBP1 mutations in early infantile epileptic encephalopathy with suppression-burst pattern. Epilepsia, doi: 10.1111/j.1528-1167.2010.02728.x.
11. Shyu AB, Wilkinson MF, van Hoof A. Messenger RNA regulation: to translate or to degrade. EMBO J 2008: 27: 471–481.
12. Maquat LE, Kinniburgh AJ, Rachmilewitz EA et al. Unstable beta-globin mRNA in mRNA-deficient beta o thalassemia. Cell 1981: 27: 543–553.
13. Wittwer CT. High-resolution DNA melting analysis: advancements and limitations. Hum Mutat 2009: 30: 857–859.
14. Dobrowolski SF, Hendrickx AT, van den Bosch BJ et al. Identifying sequence variants in the human mitochondrial genome using high-resolution melt (HRM) profiling. Hum Mutat 2009: 30: 891–898.
15. Vossen RH, Aten E, Roos A et al. High-resolution melting analysis (HRMA): more than just sequence variant screening. Hum Mutat 2009: 30: 860–866.

ARTICLE

SMOC1 Is Essential for Ocular and Limb Development in Humans and Mice

Ippei Okada,[1,14] Haruka Hamanoue,[1,2,14] Koji Terada,[3] Takaya Tohma,[4] Andre Megarbane,[5] Eliane Chouery,[5] Joelle Abou-Ghoch,[5] Nadine Jalkh,[5] Ozgur Cogulu,[6] Ferda Ozkinay,[6] Kyoji Horie,[7] Junji Takeda,[7,8] Tatsuya Furuichi,[9,10] Shiro Ikegawa,[9] Kiyomi Nishiyama,[1] Satoko Miyatake,[1] Akira Nishimura,[1] Takeshi Mizuguchi,[1,15] Norio Niikawa,[11,12] Fumiki Hirahara,[2] Tadashi Kaname,[13] Koh-ichiro Yoshiura,[12] Yoshinori Tsurusaki,[1] Hiroshi Doi,[1] Noriko Miyake,[1] Takahisa Furukawa,[3] Naomichi Matsumoto,[1,*] and Hirotomo Saitsu[1,*]

Microphthalmia with limb anomalies (MLA) is a rare autosomal-recessive disorder, presenting with anophthalmia or microphthalmia and hand and/or foot malformation. We mapped the MLA locus to 14q24 and successfully identified three homozygous (one nonsense and two splice site) mutations in the SPARC (secreted protein acidic and rich in cysteine)-related modular calcium binding 1 (*SMOC1*) in three families. *Smoc1* is expressed in the developing optic stalk, ventral optic cup, and limbs of mouse embryos. *Smoc1* null mice recapitulated MLA phenotypes, including aplasia or hypoplasia of optic nerves, hypoplastic fibula and bowed tibia, and syndactyly in limbs. A thinned and irregular ganglion cell layer and atrophy of the anteroventral part of the retina were also observed. Soft tissue syndactyly, resulting from inhibited apoptosis, was related to disturbed expression of genes involved in BMP signaling in the interdigital mesenchyme. Our findings indicate that SMOC1/Smoc1 is essential for ocular and limb development in both humans and mice.

Introduction

Microphthalmia with limb anomalies (MLA [MIM 206920]), also known as Waardenburg anophthalmia syndrome or ophthalmoacromelic syndrome, is a rare autosomal-recessive disorder first described by Waardenburg.[1] It is characterized by ocular anomalies ranging from mild microphthalmia to true anophthalmia and by limb anomalies such as oligodactyly, syndactyly, and synostosis of the 4th and 5th metacarpals.[2–4] The genetic cause for MLA has remained unknown.

It is widely known that secreted signaling molecules such as Sonic hedgehog (Shh), wingless-type MMTV integration site family (Wnt), transforming growth factor β (Tgf-β), bone morphogenetic proteins (Bmps), and fibroblast growth factor (Fgf) are involved in the development of many organs and tissues, including the eyes and limbs.[5,6] In particular, mutations in *BMP4* (MIM 112262) have resulted in anophthalmia with systemic manifestations, including polydactyly and/or syndactyly (also known as micropthalmia, syndromic 6, MCOPS6 [MIM 607932]),[7] highlighting importance of BMP signaling in both the developing eye and limb.

SMOC1 (MIM 608488), which encodes SPARC (secreted protein acidic and rich in cysteine)-related modular calcium binding 1, is a member of the SPARC (also known as BM-40) matricellular protein family that modulates cell-matrix interaction by binding to many cell-surface receptors, the extracellular matrix, growth factors, and cytokines.[8,9] SMOCs are extracellular glycoproteins with five domains: an N-terminal follistatin-like (FS) domain, two thyroglobulin-like (TY) domains, a domain unique to SMOC, and an extracellular calcium-binding (EC) domain.[9] SMOC1 is widely expressed in various tissues with localization to basement membranes.[9,10] Although the biological function of SMOC1 remains largely unknown, it has been recently reported that *Xenopus* smoc protein, the ortholog of human SMOC1, acts as a BMP antagonist,[11] suggesting that human SMOC1 can also modulate BMP signaling.

Here, we demonstrate that *SMOC1* mutations cause MLA. We also show that *Smoc1* null mice recapitulated

[1]Department of Human Genetics, Yokohama City University Graduate School of Medicine, 3-9 Fukuura, Kanazawa-ku, Yokohama 236-0004, Japan; [2]Department of Obstetrics and Gynecology, Yokohama City University Graduate School of Medicine, 3-9 Fukuura, Kanazawa-ku, Yokohama 236-0004, Japan; [3]Department of Developmental Biology, Osaka Bioscience Institute, 6-2-4 Furuedai, Suita, Osaka 565-0874, Japan; [4]Division of Pediatrics, Okinawa Prefectural Nanbu Medical Center & Children's Medical Center, 118-1 Ikyoku, Arakawa, Haebaru, Okinawa 901-1193, Japan; [5]Medical Genetics Unit, St. Joseph University, Beirut 1104-2020, Lebanon; [6]Department of Pediatrics, Ege University Faculty of Medicine, 35100 Bornova-Izmir, Turkey; [7]Department of Social and Environmental Medicine, Graduate School of Medicine, Osaka University, 2-2 Yamadaoka, Suita, Osaka 565-0871, Japan; [8]Center for Advanced Science and Innovation, Osaka University, 2-1 Yamadaoka, Suita, Osaka 565-0871, Japan; [9]Laboratory for Bone and Joint Disease, Center for Genomic Medicine, RIKEN, 4-6-1 Shirokanedai, Minato-ku, Tokyo 108-8639, Japan; [10]Laboratory Animal Facility, Research Center for Medical Sciences, Jikei University School of Medicine, 3-25-8, Nishi-Shimbashi, Minato-ku, Tokyo 105-8461, Japan; [11]Research Institute of Personalized Health Sciences, Health Sciences University of Hokkaido, Ishikari-Tobetsu, Hokkaido 061-0293, Japan; [12]Department of Human Genetics, Nagasaki University Graduate School of Biomedical Sciences, Sakamoto 1-12-4, Nagasaki 852-8523, Japan; [13]Department of Medical Genetics, University of the Ryukyus Faculty of Medicine, 207 Uehara, Nishihara, Okinawa 903-0215, Japan
[14]These authors contributed equally to this work
[15]Current address: Laboratory of Biochemistry and Molecular Biology, National Cancer Institute, National Institutes of Health, Building 37, Room 6050, Bethesda, MD 20892, USA
*Correspondence: naomat@yokohama-cu.ac.jp (N.M.), hsaitsu@yokohama-cu.ac.jp (H.S.)
DOI 10.1016/j.ajhg.2010.11.012.

MLA phenotypes, indicating that *SMOC1* plays essential roles in both eye and limb development in humans and mice.

Subjects and Methods

Subjects

A total of four families with one or two cases of MLA were analyzed in this study, including three previously reported families (A, B, and C).[12,13] Family X from Turkey, which has been previously described,[14] was newly recruited to this study. Detailed clinical information of all the patients is available in the literature,[12,14] and phenotypes of patients with confirmed mutations are summarized in Table S1 (available online). A total of five affected and 16 unaffected members from the four families were analyzed in the linkage study. Genomic DNA was obtained from peripheral-blood leukocytes with the use of QuickGene 610-L (Fujifilm, Tokyo, Japan) after informed consent had been given. Experimental protocols were approved by the institutional review board of Yokohama City University School of Medicine.

SNP Genotyping, and Fine Mapping with Short Tandem Repeat Markers

Whole-genome SNP genotyping, with the use of GeneChip Human Mapping 50K Array XbaI (Affymetrix, Santa Clara, CA), and fine mapping of possible candidate regions, with the use of additional microsatellite markers, were performed as previously described.[12,15] The list of primers used for fine mapping is presented in Table S2.

Linkage Analysis

Multipoint linkage analyses using aligned SNPs were performed with ALLEGRO software.[16] Two-point linkage analyses of candidate regions were performed with the LINKAGE package MLINK (FASTLINK software, version 5.1). In each program, an autosomal-recessive model of inheritance with complete penetrance and a disease-allele frequency of 0.001 were applied.

Mutation Analysis of Candidate Genes

All coding exons and exon-intron boundaries of *RAD51L1* (MIM 602948), *ACTN1* (MIM 102575), *ERH* (MIM 601191), *SRSF5* (MIM 600914), *DCAF5* (MIM 603812), *COX16*, *EXD2*, *GALNTL1*, *SLC39A9*, *KIAA0247*, *MED6* (MIM 602984), *TTC9* (MIM 610488), *MAP3K9* (MIM 600136), and *SMOC1* (transcript variant 1, GenBank accession number NM_001034852.1) were analyzed in the probands of families A, C, and X. The transcript variant 2 of *SMOC1* (GenBank accession number NM_022137.4) is 3 bp shorter than the variant 1, leading to an in-frame amino acid deletion at position 431. PCR was cycled 35 times at 94°C for 30 s, at 60°C for 30 s, and at 72°C for 30–90 s in a total volume of 20 μl containing 30 ng genomic DNA as a template, 0.5 μM forward and reverse primers, 200 μM each deoxyribonucleotide triphosphate (dNTP), 1 × ExTaq buffer, and 0.25 U ExTaq (Takara). All primers were designed with Primer3 software. Detailed information of primers is available upon request. PCR products were purified with ExoSAP (USB) and sequenced with BigDye Terminator 3.1 (Applied Biosystems) on a 3100 Genetic Analyzer. Sequences of patients were compared to reference genome sequences in the UCSC Genome Browser (February 2009 assembly) with Seqscape software, version 2.1 (Applied Biosystems).

Animals

Smoc1 mutant mice, created with the use of the *Sleeping Beauty* transposon system, have been previously described.[17] Line PV384 was provided by the RIKEN BioResource Center through the National BioResource Project of MEXT, Japan. Three independent mouse lines (no. 1 to no. 3), each with a single insertion in intron 1 of *Smoc1*, were bred as heterozygotes. Lines 1 and 3 were backcrossed for at least four generations to a C57BL/6J background. Line 2 was maintained with a mixed background of C57BL/6J and ICR. We mainly analyzed line 1, but we confirmed similar phenotypes in lines 2 and 3. Animals were housed in accordance with protocols approved by the Institutional Animal Care and Use Committee at Yokohama City University, School of Medicine. PCR genotyping of mice was performed with the use of genomic DNA from yolk-sac, ear, or tail biopsies. The following primers were used: PV384-WF, 5′-AAAGGCTGGGAATTGTTTG A-3′; PV384-WR, 5′-TGCAGCTGAAACTGTCTCTCC-3′; PV384-MF, 5′-TGTCCTAACTGACTTGCCAAA-3′. The PV384-WF/PV384-WR primers amplified a 441 bp wild-type (WT) product, and the PV384-MF/PV384-WR primers amplified a 218 bp mutant product.

Southern Hybridization

Genomic DNA was extracted from livers or tail biopsies of PV384 heterozygous (*Smoc1*$^{Tp/+}$) mice via standard protocols. The gene-trap insertions were analyzed by Southern hybridization with the use of 10 μg of *Sac*I-, *Nde*I-, BglII-, and *Eco*RI-digested DNA. The probe (451 bp), which hybridized to the internal ribosome entry site (IRES) in the gene-trap vector, was synthesized with the DIG PCR Probe Synthesis Kit (Roche) with the use of the following primers: 5′-CTAACGTTACTGGCCGAAGC-3′ and 5′-CCCAGATCAGATCCCATACAA-3′. Hybridization, washing, and detection of probes were performed according to the manufacturer's protocol. Images were captured with the FluorChem system (Alpha Innotech).

Cloning of Gene-Trap Insertion Sites

After identification of aberrant DNA fragments by Southern hybridization, *Nde*I-, *Sac*I-, and *Eco*RI-digested DNA from PV384 mice was fractionated by electrophoresis, and appropriately sized fragments containing *Ol1* (*other locus 1*), *Ol2*, and *Ol3* were isolated with a QIAEXII Gel Extraction Kit (QIAGEN). The isolated DNA was self-ligated by Ligation High ver.2 (Toyobo), precipitated with ethanol, and dissolved in 20 μl EB buffer (QIAGEN). Inverse PCR was performed in 25 μl reactions, containing 2 μl ligated DNA, 1 × PCR buffer for KOD FX, 0.4 mM each dNTP, 0.5 μM each primer, and 0.5 U KOD FX DNA polymerase (Toyobo). Primers common to *Ol1*, *Ol2*, and *Ol3* were as follows: Inv-F, 5′- AT CGCCAGTTCTGTATGAACGGTCTGGTCTT-3′; Inv-R, 5′-CCCTC TTTACGTGCCAGCCATCTTAGAGATAC-3′. Confirmatory PCR of gene-trap insertion sites for *Ol1*, *Ol2*, and *Ol3* loci was performed with the use of the following primers: *Ol1*-F, 5′-GAGTGGTATTCA TTGGATTCTGCTGAT-3′; *Ol2*-F, 5′-AAATCCAGCTGGCCAACAGA CTAAG-3′; *Ol3*-F, 5′-TTGCCGGGTAGACTCTATCAAGAACCA-3′; TBAL-R, 5′-CTTGTGTCATGCACAAAGTAGATGTCC-3′. Primer sets of *Ol1*-F/TBAL-R, *Ol2*-F/TBAL-R, and *Ol3*-F/TBAL-R could amplify 175 bp, 607 bp, and 767 bp products, respectively. These PCR primer pairs were also used for genotyping of mice harboring a single insertion at the *Smoc1* locus.

Confirmation of Promoter- and Poly(A)-Trapped Transcripts

Whole embryos at embryonic day 10.5 (E10.5) and E11.5 were stored in RNAlater solution (QIAGEN). Total RNA was extracted from WT, *Smoc1*$^{Tp/+}$, and *Smoc1*$^{Tp/Tp}$ embryos with the use of RNeasy Plus Mini (QIAGEN). One microgram total RNA was subjected to reverse transcription with the use of a PrimeScript 1st Strand Synthesis Kit with random hexamers (Takara). A control reaction with no reverse transcriptase was included in each experiment. PCR was performed in 20 μl reactions, containing 1 μl cDNA, 1 × PCR Buffer for KOD FX, 0.4 mM each dNTP, 0.3 μM each primer, and 0.4 U KOD FX (Toyobo). Primers used are listed below: *Smoc1*-F, 5′-GTCCCCACCTCCCCAAGTGCTTTGA-3′; *LacZ*-R, 5′-TGCCAAAAGACGGCAATATGGTGGAAA-3′; *GFP*-F, 5′-TCACATGGTCCTGCTGGAGTTCGTGAC-3′; *Smoc1*-R, 5′-ACACTTGCTCTGGCCAGCATCTTTGCAT-3′. Primer sets of *Smoc1*-F/*Smoc1*-R, *Smoc1*-F/*LacZ*-R, and *GFP*-F/*Smoc1*-R could amplify native *Smoc1* (366 bp), promoter-trapped transcripts (Tp-LacZ, 500 bp) and poly(A)-trapped transcripts (Tp-GFP, 308 bp), respectively. The PCR conditions were 98°C for 10 s, 68°C for 1 min, for 30 cycles. Primers for *ACTB*[18] were used as an internal control. PCR for *ACTB* was cycled 20 times at 94°C for 20 s, 60°C for 20 s, and 72°C for 30 s in a total volume of 10 μl containing 0.5 μl cDNA, 0.4 μM each primer, 0.2 mM each dNTP, 1 × ExTaq buffer, and 0.5 U ExTaq HS (Takara). All PCR products were electrophoresed on 2% agarose gels.

In Situ Hybridization

Embryos were collected between E9.5 and E13.5. Whole-mount in situ hybridization was carried out as previously described.[19,20] Two fragments of *Smoc1* cDNA were obtained as probes by RT-PCR, with the use of total RNA extracted from livers of E16.5 mouse embryos, and subcloned into pCR4-TOPO (Invitrogen). Primer sequences were as follows: probe 1-F, 5′-GTCTGCTCACGCCCCACT-3′; probe 1-R, 5′-CCTGAACCATGTCTGTGGTG-3′; probe P-F, 5′-CAGGAACAGGAAAGGGAAGA-3′; probe P-R, 5′-AAGGGAAAACCACACAGCAC-3′. PCR products were 1023 bp and 1578 bp, corresponding to nucleotide positions 275–1297 and 1849–3426 of the mouse *Smoc1* cDNA (GenBank accession number NM_001146217.1), respectively. The cDNA fragment amplified with probe P-F and probe P-R primers was identical to the probe used in a previous report.[21] Digoxigenin-labeled sense and antisense riboprobes were synthesized with the use of a digoxigenin RNA labeling kit (Roche). These two different antisense probes demonstrated identical staining patterns, and the control sense probes showed no staining. The expression pattern was confirmed with more than three embryos. In addition, the following probes were used: *Bmp2* (gift from Y. Takahashi),[22] *Sox9* (gift from A. Yamada),[22] *Bmp7* (gift from E.J. Robertson), and *Msx2* (gift from Dr. R.E. Maxson, Jr). The numbers of embryos examined were as follows (numerical quantity for WT, *Smoc1*$^{Tp/+}$, and *Smoc1*$^{Tp/Tp}$, respectively, shown in parentheses): *Msx2* (2, 1, 3) at E11.5; *Bmp2* (3, 0, 3), *Bmp7* (3, 0, 3), *Msx2* (3, 0, 3), and *Sox9* (2, 1, 3) at E12.5; *Bmp2* (1, 2, 3), *Bmp7* (2, 1, 3), *Msx2* (1, 2, 3), and *Sox9* (1, 3, 4) at E13.5. Stained embryos were cleared in glycerol to enable images to be produced with a VHX-1000 digital microscope (Keyence).

Histology

Heads of embryos and newborns were fixed overnight in 4% paraformaldehyde in PBS at 4°C. These embryos were then washed in PBS. Frozen samples were serially sectioned at 16 μm (E14.5) and 20 μm (P0). The numbers of eyes examined (WT, *Smoc1*$^{Tp/+}$, *Smoc1*$^{Tp/Tp}$) were as follows: coronally sectioned at E14.5 (8, 10, 12), coronally sectioned at P0 (8, 10, 6), horizontally sectioned at P0 (2, 2, 4). For evaluation of ventral atrophy of the retina, only the coronally sectioned eyes were used. TB staining was performed according to standard protocols. Forelimbs of mice were fixed in 4% paraformaldehyde in PBS, decalcified in 10% EDTA, and embedded in paraffin. Forelimbs were serially sectioned at 4 μm and stained with hematoxylin and eosin.

Evaluation of Optic Nerve Diameter

The palatine and orbital bones were carefully removed to expose the optic chiasm and optic nerve. During the dissection process, 4% paraformaldehyde in PBS was frequently applied onto the gaps between the bone and optic nerve. Xylene cyanol was applied to enhance the outline of optic nerves at poastnatal day 0 (P0). Photographs of optic nerves were taken with a VHX-1000 digital microscope, and the diameter was measured for right and left optic nerves with the bundled software included with the VHX-1000 instrument.

Skeletal Staining

For skeletal preparations, mice were fixed in 99.5% ethanol after removal of the skin and viscera. Cartilage tissues were stained with 0.015% alcian blue and 20% acetic acid in 75% ethanol for three days at 37°C. After dehydration with 99.5% ethanol for three days, bones were stained with 0.002% alizarin red in 1% KOH. Then skeletons were cleared in 1% KOH for several weeks. For P14 mice, soft tissues were dissolved in 2% KOH before alizarin red staining.

Nile Blue Staining

For the study of apoptosis of hindlimbs at E13.5 and E14.5, Nile blue (NB) staining was performed on the basis of a previously described protocol,[23] except that staining was performed at 37°C (not room temperature). Apoptosis was determined by NB-stained (deceased) cells. After rinsing in Tyrode solution, hindlimbs of control (WT and heterozygous littermates) and homozygous mice were evaluated. Photographs of dorsal aspects were taken with a VHX-1000 digital microscope. Experiments were repeated three times, and reproducible representative results are presented.

Statistical Analysis

Statistical analyses were performed with the use of non-repeated-measures ANOVA followed by Dunnett's post hoc test. The results are given as mean ± standard deviation, and the threshold p value for statistical significance was 0.01.

Results

Identification of Homozygous *SMOC1* Mutations

We have previously mapped the MLA locus to a 422 kb region at 10p11.23 by analyzing three families (one Japanese family [A] and two Lebanese families [B and C]). This region contained only one gene, *MPP7*, in which no mutations were found.[12] After a new Turkish family (X) was added to the analysis, the MLA locus was again searched by homozygosity mapping to the consanguineous families (X, B, and C) and haplotype mapping to family A for detection of compound-heterozygous mutations; however, we could not detect any common regions

among the four families. We then focused on identifying common regions in any three of the four families to allow for locus heterogeneity (Table S3).

A locus at 14q24.1-q24.2, which showed the highest LOD score (3.936) among the candidate regions larger than 2.0 Mb, was highlighted among families A, C, and X. This locus was analyzed with the use of additional microsatellite markers, and a 3.0 Mb region containing 24 genes was identified (Figures 1A and 1B). A total of 14 genes were sequenced, and homozygous mutations were found in *SMOC1*: c.718C>T (p.Gln240X) in family A, c.664+1G>A in family C, and c.378+1G>A in family X (Figures 1C and 1D). All of these homozygous mutations were cosegregated with the disease phenotype, and the parents of the individuals with these mutations were heterozygous carriers (Figure 1C). We could not find any mutations in *SMOC1* in family B, in which MLA is unlinked to the 14q24.1-q24.2 locus. Interestingly, in family A haplotypes of paternal and maternal alleles, each having the same mutation, are completely different (data not shown), suggesting that the same mutation may have occurred in separate events. The c.718C>T mutation was not detected in 289 healthy Japanese controls, including 100 Okinawa islanders. The other two mutations were not detected in ethnically matched controls (54 Lebanese and 99 Turkish subjects, respectively), nor in 289 Japanese controls. The two splice-donor-site mutations (c.664+1G>A and c.378+1G>A) are predicted to abolish a donor site, as predicted by ESEfinder, NetGene2, HSF2.4.1, SpliceView, and BDGP analysis (Table S4). Thus, the three mutations are likely to lead to a loss of functional SMOC1.

Smoc1 Expression in the Developing Eye and Limb in Mice

For the examination of *Smoc1* expression in the developing eye and limb, whole-mount in situ hybridization of mouse embryos was performed. *Smoc1* was expressed in the forebrain, midbrain, hindbrain, pharyngeal arch, somites, and forelimb buds at E9.5 (Figure 2A). At E10.5, *Smoc1* expression was observed in the optic stalk (Figure 2B), and at E11.5, expression was localized to the closure site of the optic cup (Figure 2C). Expression of *Smoc1* in developing limbs between E10.5 and E11.5 was observed in both dorsal and ventral regions, with a broader pattern of expression in dorsal regions, but expression was not detected in the most anterior, posterior, and distal parts of limb buds (Figures 2D and 2E). Expression coinciding with chondrogenic condensation was observed at E12.5 (Figure 2F), and expression then became restricted to future synovial joint regions at E13.5 (Figure 2G). This dynamic expression suggests that *Smoc1* plays a critical role in ocular and limb development.

Ocular and Limb Anomalies in *Smoc1* Null Mice

To investigate the pathological basis of MLA due to the loss of *SMOC1* function, we obtained *Smoc1* mutant mice, PV384.[17] PV384 mice possess gene-trap insertions in the *Smoc1* locus and in three other loci. After PV384 mice were bred with C57BL/6J or ICR mice, we obtained three independent lines (no. 1 to no. 3), each with a sole insertion in intron 1 of *Smoc1* (Figure S1). We mainly analyzed line 1, but we confirmed similar phenotypes in lines 2 and 3. Heterozygous mutant mice ($Smoc1^{Tp/+}$) were healthy and fertile. Homozygous mice ($Smoc1^{TP/TP}$) were null mutants, as they showed no native transcript of *Smoc1* (Figure S1E). Homozygous mice were viable at P0; however, they did not survive beyond the first 3 wks of life (Figure 3B). Their growth was retarded in comparison to WT and heterozygous littermates at P0 and P14 (Figures 3A and 3C). Developmental defects in eyes and optic nerves were evident at E14.5. Homozygous mice had relatively small eyes, and histological examinations revealed aplasia or hypoplasia of optic nerves (in 10 of 12 optic nerves), atrophy of the anteroventral part of the retina (in 11 of 12 eyes), and extension of the retinal pigmented epithelium (RPE) to the optic nerve (in 10 of 12 eyes) (Figures 3D–3I). These abnormalities were also observed at P0 (aplasia or hypoplasia of optic nerves [in 7 of 10 optic nerves], retinal atrophy [in 6 of 6 eyes], and RPE extension [in 3 of 6 eyes with identifiable optic nerves]) (Figures 3J–3M). WT or heterozygous littermates did not show any such abnormalities, except that a few eyes of heterozygous mice showed extension of the RPE at E14.5, but not at P0 (in 2 of 10 and 0 of 12 eyes, respectively). Toluidine blue (TB) staining showed ganglion cell layers that were thinned and irregular to varying degrees in homozygous mice, suggesting a reduced number of retinal ganglion cells (Figures 3J–3K′). Thus, *Smoc1* is required for axon sprouting, elongation, or maintenance of retinal ganglion cells.[24] Hypoplasia of optic nerves was further quantitatively confirmed by macroscopic examination: the average diameter of optic nerves of homozygous mice was significantly smaller than that of WT and heterozygous littermates at P0 and P14 (Figures 3L–3Q). These data clearly demonstrate that loss of *Smoc1* in mice affects development of the body, retina, and optic nerves, in a manner similar to that seen in MLA patients.[3,4]

Newborn homozygous mice could be readily identified by their hindlimb syndactyly and pes valgus, whereas no abnormalities were observed in WT and heterozygous pups (Figure 4 and Table 1). Interestingly, the severity of syndactyly varied between mouse lines: line 1 exclusively showed soft tissue syndactyly, whereas line 2 frequently showed four digits (Figures 4F and 4J). Skeletal preparations with alcian blue and alizarin red revealed that the foot with four digits had four phalanx and five metatarsals with fusion to each other (Figure 4K). Thus the *Smoc1* null mutation resulted in a spectrum of phenotypes, from soft tissue syndactyly to four fused digits, probably due to different genetic backgrounds. Bowed tibiae and hypoplastic fibulae were also consistently observed in homozygous mice (Figures 4H and 4L). The articulation between

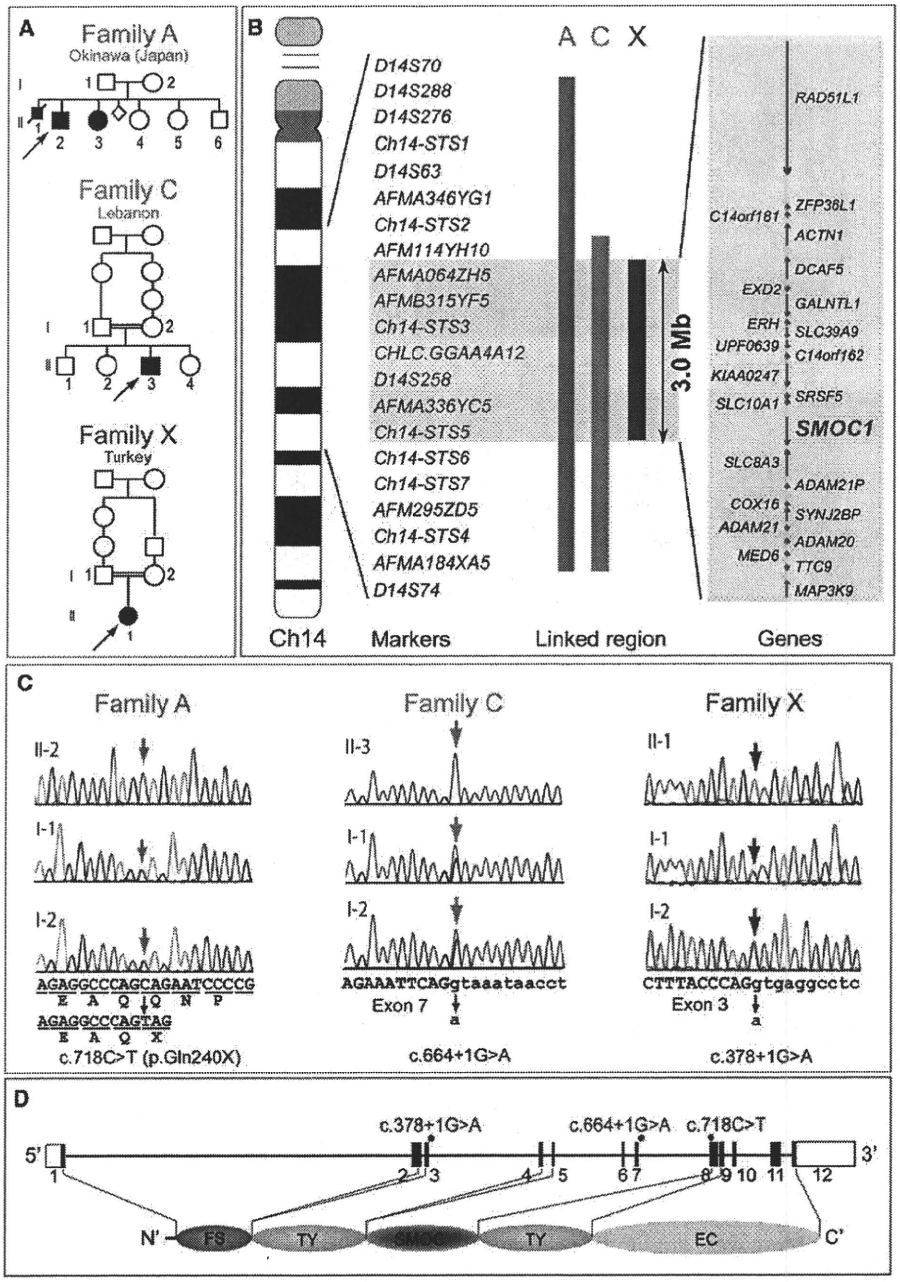

Figure 1. Genetic Analysis of Three Families with Members Affected by Microphthalmia with Limb Anomalies

(A) Pedigrees of the three families.

(B) Linkage analysis with SNPs and microsatellite markers on chromosome 14. From left to right: chromosome ideogram, genetic markers, linked regions of the three families, and genes mapped to the shortest overlapping linked region (between *AFM114YH10* and *Ch14-STS6* [UCSC coordinates, Feb. 2009: chromosome 14: 68,388,190–71,347,908 bp]).

(C) Sequences of mutations identified in each family. Affected patients in family A have a homozygous nonsense mutation (c.718C>T). Patients in families C and X have distinct homozygous splice-donor site mutations (c.664+1G>A and c.378+1G>A, respectively). For all mutations, parents of affected patients are heterozygous carriers, without exception. Sequences of the exon and intron are presented in upper and lower cases, respectively.

(D) At the top is a depiction of a schematic representation of *SMOC1* consisting of 12 exons (UTR and coding exons are indicated by open and filled rectangles, respectively). The locations of three mutations are indicated by red dots. At the bottom, the functional domains of SMOC1 are depicted. Abbreviations are as follows: FS, the follistatin-like domain; TY, the thyroglobulin-like domain; SMOC, the domain unique to SMOC; and EC, the extracellular calcium-binding domain.

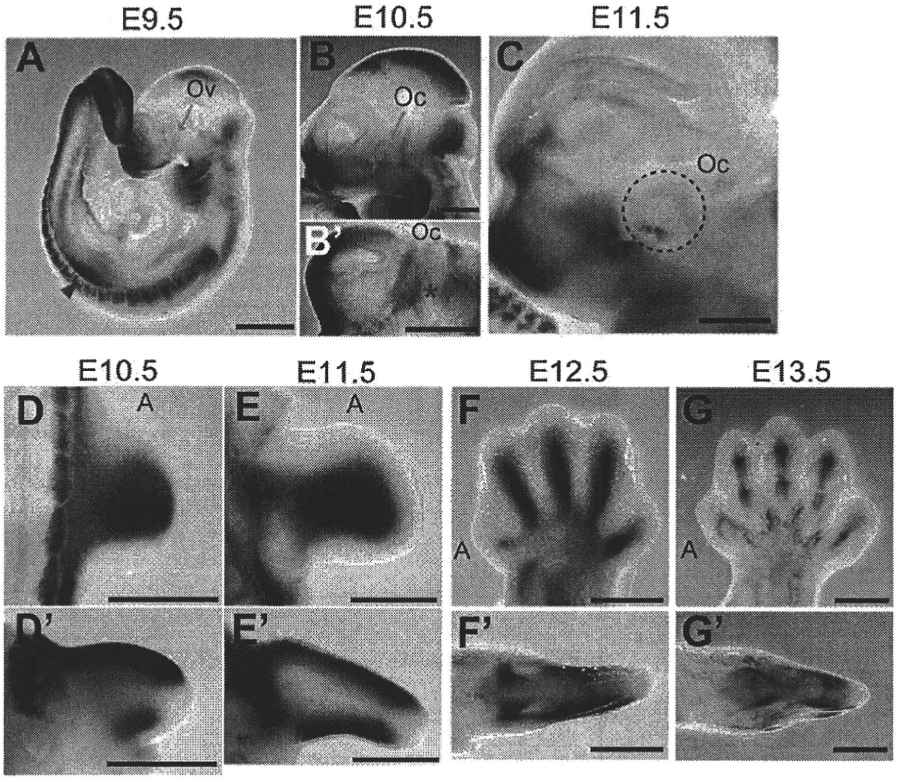

Figure 2. *Smoc1* Expression in Mouse Embryos
Lateral views of embryos (A–C) and a ventral view of the left part of the head (B′, lateral view is shown at the top).
(A) At E9.5, *Smoc1* was expressed in the forebrain, midbrain, hindbrain, pharyngeal arch, somites, and forelimb buds (magenta arrowhead), but not in the optic vesicle (Ov, blue arrow).
(B and B′) Expression in the optic stalk became evident at E10.5 (magenta asterisks), but was not evident in the optic cup (Oc, blue arrow).
(C) Expression was restricted to the closure site of the optic cup (dashed circle) at E11.5.
(D–G) Dorsal and (D′–G′) posterior view of the right hindlimbs (dorsal view is shown at the top in D′–G′). The anterior side is indicated by an A. (D and D′) At E10.5, *Smoc1* was more widely expressed in the dorsal part of the limb bud than in the ventral part. *Smoc1* expression is undetected in the most anterior, posterior, and distal parts of the limb bud. (E and E′) At E11.5, ventral expression was broader than that in the previous stage. (F and F′) At E12.5, expression was detected in areas consistent with chondrogenic condensation. (G and G′) At E13.5, *Smoc1* expression became restricted to future joint regions. Scale bar represents 500 μm.

tibia/fibula and calcanea of homozygous mice appeared malpositioned (Figures 4G and 4K), which might contribute to pes valgus. At P14, soft tissue syndactyly was also evident in most forelimbs of homozygous mice (Figures 4M–4O). Moreover, hindlimbs of homozygous mice showed synostosis between the 4^{th} and 5^{th} metatarsals (Figure 4T), which is observed in both the hands and the feet of MLA patients. Thus, many limb anomalies of MLA patients were recapitulated in *Smoc1* null mice (Table S1).

Reduced Interdigital Apoptosis and Disturbed BMP Signaling

Among the various abnormalities caused by loss of *Smoc1* function, we focused on soft tissue syndactyly, which was commonly observed in both fore- and hindlimbs of null mutants. It is possible that the syndactyly is caused by failed apoptotic regression of the interdigital mesenchyme. To examine this hypothesis, hindlimbs were stained with NB sulfate at E13.5 and E14.5, the time when interdigital apoptosis is most evident. In control embryos (WT and heterozygous littermates), NB-stained apoptotic cells were identified in the interdigital mesenchyme, where regression of the interdigital webbing occurs in the distal region (Figures 5A and 5C). By contrast, the number of apoptotic cells in the mesenchyme between digits 2 and 3 and digits 3 and 4 was dramatically reduced in homozygous mice at E13.5 and E14.5, along with persistent webbing in the distal region (Figures 5B and 5D, magenta asterisk). BMP signaling is involved in apoptosis of the interdigital mesenchyme.[25,26] *Bmp2*, *Bmp7*, and *Msx2*, a direct target of BMP signaling, were strongly expressed in the interdigital mesenchyme of control hindlimbs at both E12.5 and E13.5. However, the expression of these three genes was profoundly reduced and perturbed in hindlimbs of homozygous mice (Figures 5E–5J). These data suggest that inhibition of apoptosis is spatiotemporally correlated to reduced and/or disturbed expression of genes involved in BMP signaling in the interdigital mesenchyme.